

7-1-2016

Reconstructing the historical Albuquerque reach of the Middle Rio Grande to evaluate the influence of river engineering on floodplain inundation

Jourdan Adair

Follow this and additional works at: https://digitalrepository.unm.edu/ce_etds

Recommended Citation

Adair, Jourdan. "Reconstructing the historical Albuquerque reach of the Middle Rio Grande to evaluate the influence of river engineering on floodplain inundation." (2016). https://digitalrepository.unm.edu/ce_etds/121

This Thesis is brought to you for free and open access by the Engineering ETDs at UNM Digital Repository. It has been accepted for inclusion in Civil Engineering ETDs by an authorized administrator of UNM Digital Repository. For more information, please contact disc@unm.edu.

Jourdan Brittani Marie Adair

Candidate

Civil Engineering

Department

This thesis is approved, and it is acceptable in quality and form for publication:

Approved by the Thesis Committee:

Dr. Mark Stone, Chair

Dr. Ricardo González-Pinzón

Todd Caplan

**RECONSTRUCTING THE HISTORICAL ALBUQUERQUE REACH OF THE
MIDDLE RIO GRANDE TO EVALUATE THE INFLUENCE OF RIVER
ENGINEERING ON FLOODPLAIN INUNDATION**

by

JOURDAN BRITTANI MARIE ADAIR

B.S., CIVIL ENGINEERING, UNIVERSITY OF NEW MEXICO, 2014

THESIS

Submitted in Partial Fulfillment of the
Requirements for the Degree of

Master of Science

Civil Engineering

The University of New Mexico
Albuquerque, New Mexico

July, 2016

Acknowledgements

This research is supported by the National Science Foundation (NSF) under Grant No. CBET-1254569. NSF saw the potential in the idea of one person, Dr. Mark Stone, who deserves more than a thank you. A coincidence in classroom location turned into six years of advisement, mentorship, and friendship. Thank you for introducing me to the world of water. To Colin, my seemingly unending questions were only outmatched by your unending willingness to help. Thank you for providing modeling results and for being the cornerstone of the Flood Group.

I would also like to thank my committee members, Dr. Ricardo González-Pinzón and Todd Caplan, for their continued support, as well as Chad McKenna at GeoSystems Analysis, Inc. and Jonathan AuBuchon at the Bureau of Reclamation, Albuquerque Area Office for providing all of the data on which this project is based.

Finally, to my parents, thank you for always setting the bar high and never letting me settle for anything less. Those expectations pushed me to the finish line. And to the Joshua's in my life, I cannot wait to have you both by my side on that big day in July.

**Reconstructing the historical Albuquerque reach of the Middle Rio Grande to evaluate
the influence of river engineering on floodplain inundation**

by

Jourdan Brittani Marie Adair

B.S., Civil Engineering, University of New Mexico, 2014

M.S., Civil Engineering, University of New Mexico, 2016

ABSTRACT

Sustainable floodplain management is essential in achieving a balance between population growth and natural resource protection, especially in the face of climate change. While floodplain development in the Middle Rio Grande Valley has allowed for economic expansion in the region, it has come at a cost to the fragile ecosystem of the Southwest. In this study, the historical Albuquerque reach of the Middle Rio Grande is reconstructed, including floodplain topography, channel characteristics, and land cover from approximately 1918. The impacts of river engineering on flooding events are evaluated by comparing historic and current conditions. Hydrodynamic modeling is first used to quantify the effects, then results are analyzed by calculating inundated area and visualized with inundation mapping. Model results show a decrease in inundated area, accompanied by a rise in flood stage. This has implications for both sides of the human-

environment interface and identifies the need for rebuilding system resiliency and restoring connectivity.

Table of Contents

List of Figures	vii
List of Tables	ix
1 Introduction	1
1.1 Study Reach and Objectives.....	1
1.2 Research Implications	2
2 Literature Review	3
2.1 Impacts of Engineering Modifications on River Systems	3
2.2 Historical Reconstruction and Evaluation of River Channel Changes	6
2.3 Middle Rio Grande	7
3 Data Collection	8
3.1 Historical Data.....	8
3.2 Current Data	11
4 Geospatial Reconstruction Methods	11
4.1 Floodplain Topography	11
4.2 Channel Characteristics.....	14
4.3 Land Cover	18
5 Hydrodynamic Modeling	21
5.1 Model Selection and Development.....	22
5.2 Mesh Refinement and Parallelization	22
5.3 Flow Conditions	23
6 Results	23
6.1 Geospatial Inputs	23
6.2 Inundated Area and Inundation Mapping.....	28
6.3 Velocity Relative Frequency Histograms.....	38
7 Discussion	40
8 Conclusion	44
Appendices	45
Appendix A: Historical Photography	45
Appendix B: Map and Plots of SCS Survey Lines	47
Appendix C: MATLAB Code	51
Appendix D: 2D Hydrodynamic Modeling with D-Flow Flexible Mesh	53
References	55

List of Figures

Figure 1: Timeline of historical activities impacting the Rio Grande near Albuquerque, NM (modified from Swanson et al., 2011).	8
Figure 2: Estimated SCS survey line locations and Rio Grande bank lines shown within the boundary of the study reach AOI. Basemap is the 1935 aerial photography from USBR.	10
Figure 3: Study reach location with bank lines and contour lines extracted from the 1918 digitized maps.	13
Figure 4: Schematic (i.e., not actual data) of the formatting process for HEC-RAS cross-section creation within GIS: (a) cutline digitized, bank points identified by coordinates, and elevations extracted from the floodplain terrain; (b) SCS channel survey line as XYZ points; (c) channel bathymetry merged with floodplain terrain between bank points.....	16
Figure 5: RAS Mapper view of the study reach AOI showing cross-sections imported from GIS at each SCS survey line location and cross-sections interpolated using HEC-RAS.....	17
Figure 6: Land cover classifications within the AOI of the study reach.....	25
Figure 7: Retro-DEM displayed with hillshade.	26
Figure 8: Expanded view of three sub-areas showing the retro-DEM in greater detail...	27
Figure 9: Inundation map for historic conditions at a flow of $142 \text{ m}^3/\text{s}$ (5,000 cfs).....	30
Figure 10: Inundation map for historic conditions at a flow of $283 \text{ m}^3/\text{s}$ (10,000 cfs)....	31
Figure 11: Inundation map for historic conditions at a flow of $425 \text{ m}^3/\text{s}$ (15,000 cfs)....	32
Figure 12: Inundation map for historic conditions at a flow of $566 \text{ m}^3/\text{s}$ (20,000 cfs)....	33
Figure 13: Inundation map for modern conditions at a flow of $142 \text{ m}^3/\text{s}$ (5,000 cfs).....	34
Figure 14: Inundation map for modern conditions at a flow of $283 \text{ m}^3/\text{s}$ (10,000 cfs)...	35
Figure 15: Inundation map for modern conditions at a flow of $425 \text{ m}^3/\text{s}$ (15,000 cfs)...	36
Figure 16: Inundation map for modern conditions at a flow of $566 \text{ m}^3/\text{s}$ (20,000 cfs)...	37
Figure 17: Distribution of velocities for the historic and modern models at a flow of $142 \text{ m}^3/\text{s}$ (5,000 cfs).	38
Figure 18: Distribution of velocities for the historic and modern models at a flow of $283 \text{ m}^3/\text{s}$ (10,000 cfs).	39
Figure 19: Distribution of velocities for the historic and modern models at a flow of $425 \text{ m}^3/\text{s}$ (15,000 cfs).	39
Figure 20: Distribution of velocities for the historic and modern models at a flow of $566 \text{ m}^3/\text{s}$ (20,000 cfs).	40
Figure 21: Central Avenue Bridge on May 26, 1930 (from Daves, 1994).	45
Figure 22: Submerged area five miles north of Socorro, N.M. (from Bloodgood, 1930). 45	
Figure 23: Waterlogged Middle Rio Grande Valley in 1928. Photo taken in Albuquerque near Rio Grande Blvd NW, north of I-40 (from MRGCD, 2009).	46
Figure 24: Map of the SCS cross-section range lines located within the Middle Rio Grande Valley, including two range lines in the study reach: 903.4 and 907.6 (from Happ, 1948).	47

Figure 25: "Below Alameda Bridge" SCS range line obtained from USBR.....	48
Figure 26: "Above Highway 66 Bridge" SCS range line obtained from USBR.....	48
Figure 27: "Below Highway 66 Bridge" SCS range line obtained from USBR.	49
Figure 28: "903.4" SCS range line obtained from USBR.	49
Figure 29: "Below Highway 85 Bridge" SCS range line obtained from USBR.	50
Figure 30: "907.6" SCS range line obtained from USBR.	50
Figure 31: USGS gage data for the 1942 flood used for modeling (from USGS, 2016). ...	53

List of Tables

Table 1: SCS survey lines and year surveyed.....	9
Table 2: Examples of vegetation types shown on the 1918 topo maps.....	18
Table 3: Examples of soil types, land uses, and markers shown on the 1918 topo maps.	18
Table 4: Land cover classifications and corresponding Manning's n values.	21
Table 5: Comparison of inundated area for the historic and modern models under four flow conditions.	28
Table 6: Comparison of percent inundation located in the channel versus the floodplain for the historic and modern models at each flow condition.....	29
Table 7: Comparison of mean daily discharges for the Rio Grande before (1943-1974) and after (1974-1995) construction of Cochiti Dam (modified from Richard and Julien, 2003).	42

1 Introduction

1.1 Study Reach and Objectives

Large-scale modifications to the Rio Grande began in 1925, following the formation of the Middle Rio Grande Conservancy District (MRGCD), with the purpose of protecting agricultural areas and developing communities in the Middle Rio Grande Valley from flooding and a rising water table (MEI, 2002a). The study reach is approximately 35 river kilometers (22 river miles) of the Middle Rio Grande, extending from Alameda Bridge to Isleta Diversion Dam. Referred to as the “Albuquerque reach” due its proximity to the City of Albuquerque, the reach has a long history of human modification. River engineering techniques included construction of diversion dams for sediment and flood-control, jetty jacks for channel stabilization, and levees for river straightening. The objective of this study is to reconstruct the historical Rio Grande to evaluate how river engineering has influenced the movement of flood waves through the Albuquerque reach. This project focuses on reconstructing Rio Grande channel conditions prior to the MRGCD using limited historical data from 1918 to 1937. While adjustments in channel planform and morphology have been previously analyzed along various reaches of the Middle Rio Grande (e.g., Massong, 2010; Owen, 2012; Salazar, 1998; Swanson et al., 2011), evaluating the combined changes in channel morphology, floodplain topography, and land cover provide a uniquely holistic perspective of historical river engineering effects. Comparing hydrodynamic modeling results from the resultant historical surface with those from a model of current conditions allows for

quantification of how river engineering has influenced the movement of floods through the Albuquerque reach. Ultimately, this “retro-model” (Remo and Pinter, 2007) built from historical data serves as a reference condition for the development of more sustainable flood protection strategies and improved river management policies.

1.2 Research Implications

River engineering on the Middle Rio Grande has disconnected the river from its floodplain, resulting in modifications to natural processes and a subsequent loss of channel-floodplain connectivity. Any amount of connectivity lost due to channel constraint can significantly reduce the important role that floodplains play in providing ecological benefits and ecosystem services, such as nutrient exchange, habitat availability, and flood risk reduction (Jacobson et al., 2015; Remo et al., 2012). Flood risk reduction is becoming an increasingly important issue as climate change threatens to intensify flooding and rapid urbanization increases flood vulnerability (Zhu et al., 2007). Combined with the hazard of aging flood-control infrastructure, this necessitates floodplain management strategies that focus on boosting system resiliency. As a result, the need exists to find a balance between maximizing river-floodplain connectivity, restoring flood wave attenuation as an environmental service, and minimizing the risk of flooding to agricultural fields and communities within the floodplain.

Modeling how river engineering affects the movement of floods is one way to achieve more sustainable flood protection strategies by identifying and optimizing areas that have the greatest potential for restoration. Increasing knowledge of river-floodplain

interactions and historical engineering effects is becoming increasingly important in defining modern water policy (Hohensinner et al., 2003). These issues are recognized globally, with considerable action being taken in the Netherlands to implement a more sustainable and integrated approach to flood defense that includes making room for the river through changing land-use and reclaiming the floodplain with levee setbacks (Hein et al., 2005; Rijke et al., 2012). As new policies are enacted and the approach to water management continues to evolve, it will only become more imperative to evaluate and better understand the interactions between natural and engineered environments.

2 Literature Review

2.1 Impacts of Engineering Modifications on River Systems

At the interface between natural and built environments lies an increasingly complex dynamic between human consumption and resource depletion. As development in high-risk areas such as floodplains continues, modifications to the floodplain and river are made in order to support rising populations and protect infrastructure from flooding. Along with the effects of climate change, these human activities remain a threat to hydrologic processes. Perhaps the most severe consequence of anthropogenic intervention is the observed increase in flood magnitude and variability (Pinter et al., 2010; Vorogushyn and Merz, 2013). Flood magnification over time can be attributed to mechanisms from three categories: (1) climate change, (2) land-use change, and (3) river engineering (Bormann et al., 2011; Pinter and Heine, 2005).

Past studies on the Mississippi River and the Lower Missouri River have focused on the third category, with the construction of structures such as wing dikes, bendway weirs, levees, meander cutoffs, lock-and-dams, and bridges (Bormann et al., 2011; Pinter et al., 2010). Pinter and Heine (2005) used a specific-gage analysis to evaluate flood magnification on the Lower Missouri River as a result of river regulation activity, while Pinter et al. (2010) used a statistical model with variables developed from the specific-gage technique to test the effects of historical modifications on changes in flow trends on both the Mississippi and Missouri Rivers. Specific-gage analysis isolates the effects of river engineering by holding discharge constant through time and quantifying changes in the stage-discharge relationship. This is particularly useful for identifying causation since peak discharge trends are more reflective of climate or land-use changes, while trends in flood heights more directly reflect the effects of in-stream engineering (Bormann et al., 2011). Pinter et al. (2010) found results to be dependent on flow and reach-specific conditions. For example, upstream levees on the Middle Mississippi reach decreased stages for flows below bankfull, but increased stages for flood flows (Pinter et al., 2010). The strongest correlation was found on the Lower Mississippi reach, where downstream meander cutoffs were associated with reducing stage by up to 3.8 m, most likely due to channel incision occurring downstream after cutoff completion (Pinter et al., 2010). Consistent with this thought is the opposite situation on the Lower Missouri River, in which cutoffs upstream caused aggradation downstream and therefore a rise in stage (Pinter et al., 2010). Construction of wing-dikes, on the other hand, increased stage upstream due to back-water effects across all

flow conditions on the Middle Mississippi River (Pinter et al., 2010). Even though a systemwide model was also performed, Pinter et al. (2010) concluded that models at the reach-scale were more representative of the system due to the inability of the systemwide model to address heterogeneity within the individual reaches and overlap between them.

Hydrologic response to engineering modifications has gained international attention, particularly in Germany, where the Rhine has undergone extensive river training, resulting largely from a rapid growth in population within the last 200 years (Bormann et al., 2011). In terms of amplified flood peaks, Vorogushyn and Merz (2013) found river engineering to be a significant contributor to increasing flood trends along the Rhine, causing a decrease in flood wave attenuation. Bormann et al., (2011) employed the specific gage analysis at 78 gages on 26 German rivers and found results to be highly variable at this much larger scale. While both increasing and decreasing trends were found for stage and discharge, only about 30% of the gages showed statistically significant trends, indicating that the effects of river engineering on the three metrics analyzed were overall less significant on German rivers than on rivers studied in the U.S. (Bormann et al., 2011).

2.2 Historical Reconstruction and Evaluation of River Channel Changes

Historical reconstruction is a useful tool in evaluating river channel changes over time. Knowledge gained through evaluating historical changes can improve the management of rivers and floodplains and the development of flood protection strategies (Bormann et al., 2011). Methods of historical reconstruction include examining aerial photography and digitizing channel characteristics using a geographic information system (GIS) software. A more detailed analysis can be done with the use of topographic data for representing floodplain topography as well as cross-section data for describing morphology of the main channel. Paz et al. (2010) developed an automated GIS procedure for preparing geometric data for input into the Hydrologic Engineering Center's River Analysis System (HEC-RAS), a hydraulic modeling software from the United States Army Corps of Engineers (USACE). The procedure combined channel survey data with floodplain elevation data from a digital elevation model (DEM) to produce cross-sections that encompassed both the main channel and floodplains. Due to the relatively coarse spacing of available channel cross-section surveys, a linear interpolation procedure was used to interpolate cross-sectional profiles between known cross-sections (Paz et al., 2010). Model results indicated that this GIS procedure was successful in overcoming the challenges of modeling a large river network with limited data availability. The approach of this study is similar to the procedure developed in this project, confirming the use of GIS and automation as an acceptable approach for building model inputs with a data set from a variety of sources and formats.

2.3 Middle Rio Grande

The Middle Rio Grande Valley, from Cochiti Dam to Elephant Butte Dam, is as diverse in its use as it is its ownership. This presents a unique challenge in managing the Rio Grande, an already limited resource that supports life within the region. Figure 1 gives a timeline of the major activities affecting the Rio Grande near Albuquerque, New Mexico. These activities, dating back to the late 1800s, range from agricultural practices within the floodplain to river engineering projects. Records reveal periods of large flooding occurred throughout the Middle Rio Grande in the late 1920s, 1930s, and early 1940s (MEI, 2002a). Following extreme flooding and waterlogging (See Appendix A), measures were taken to protect farmland in the valley by constructing levees for channelization in the 1920s and 1930s then installing Kellner jetty jacks for bank stabilization in the 1940s to 1960s (Swanson et al., 2011). From 1916 to 1975, major flood control and irrigation diversion dams were constructed on the Rio Grande and its tributaries, including five dams on the main stem of the Middle Rio Grande: Elephant Butte Dam, Angostura Diversion Dam, Isleta Diversion Dam, San Acacia Diversion Dam, and Cochiti Dam. Because the reach is centered on the City of Albuquerque, rapid development, and accompanying land use changes, have significantly modified the valley since the 1940s (Swanson et al., 2011). This combination of channel constraint and flow regulation from river engineering has resulted in distinct channel planform changes for the Rio Grande, including a significant decrease in channel width, as evaluated by a number of researchers (e.g., Bauer, 2000; Leon et al., 2009; Swanson et al., 2011).

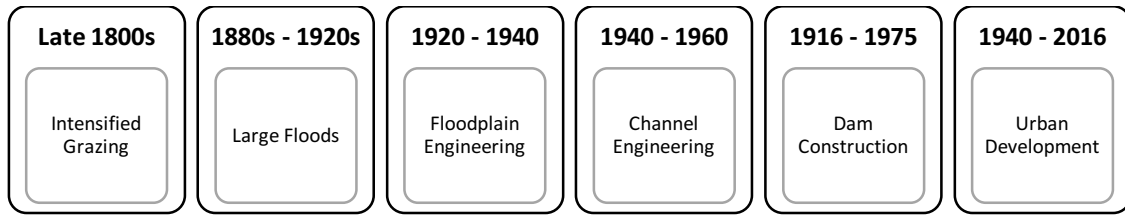


Figure 1: Timeline of historical activities impacting the Rio Grande near Albuquerque, NM (modified from Swanson et al., 2011).

3 Data Collection

Geospatial data, including floodplain topography, channel bathymetry, and land cover, were compiled from various sources. The combination of these data is extremely important in accurately modeling the routing of floods and river hydraulics along the reach (Paz et al., 2010). These inputs were used to reconstruct the historical digital elevation model (DEM), or "retro-DEM" (Remo and Pinter, 2007), representing the Rio Grande circa 1918.

3.1 Historical Data

The retro-DEM contains data from historical maps and surveys. A 1918 topographical map set, published by the U.S. Reclamation Service in 1922, was georeferenced and digitized by the U.S. Bureau of Reclamation (USBR) Denver office using GIS. The set includes a total of 34 sheets at a scale of 1:12,000 and contains topographic and land cover data for the Middle Rio Grande Valley between White Rock Canyon and San Marcial. While the upstream boundary of the study reach, Alameda Bridge, is identifiable, the downstream boundary, Isleta Diversion Dam, had to be located using geographic coordinates as the dam was not opened until 1934 and is therefore not

shown on the map. As for channel characteristics, historical survey data from USBR includes cross-section surveys taken at Soil Conservation Service Range Lines (SCS survey lines). These lines were surveyed in 1936 and 1937 and are numbered according to Santa Fe Railway railroad mileage (Bauer, 2000). While these survey lines capture general characteristics such as the width of the channel and variability of the channel bottom, the historical Rio Grande is highly dynamic, meaning the surveys were interpreted as a single snapshot in time rather than a steadfast representation of the system.

Aerial photographs from 1935 (Figure 2) also helped in reconstructing the historic channel; however, in comparison to the 1918 map set, there is an obvious shift in planform between 1918 and 1935. For modeling purposes, the spatial extent of the available survey lines further constrained the study reach to an area of interest (AOI) ranging from approximately 0.2 river miles downstream of Alameda Bridge (Bauer, 2000) to south of Highway 85 Bridge, known currently as New Mexico State Road 314 or Bridge Boulevard SW. Table 1 summarizes the SCS survey line names and the year in which they were surveyed, while Figure 2 maps the survey lines located within the AOI.

Table 1: SCS survey lines and year surveyed.

SCS Survey Line	Below Alameda Bridge	Above Highway 66 Bridge	Below Highway 66 Bridge	903.4	Below Highway 85 Bridge	907.6
Year	1936	1936	1936	1937	1936	1937

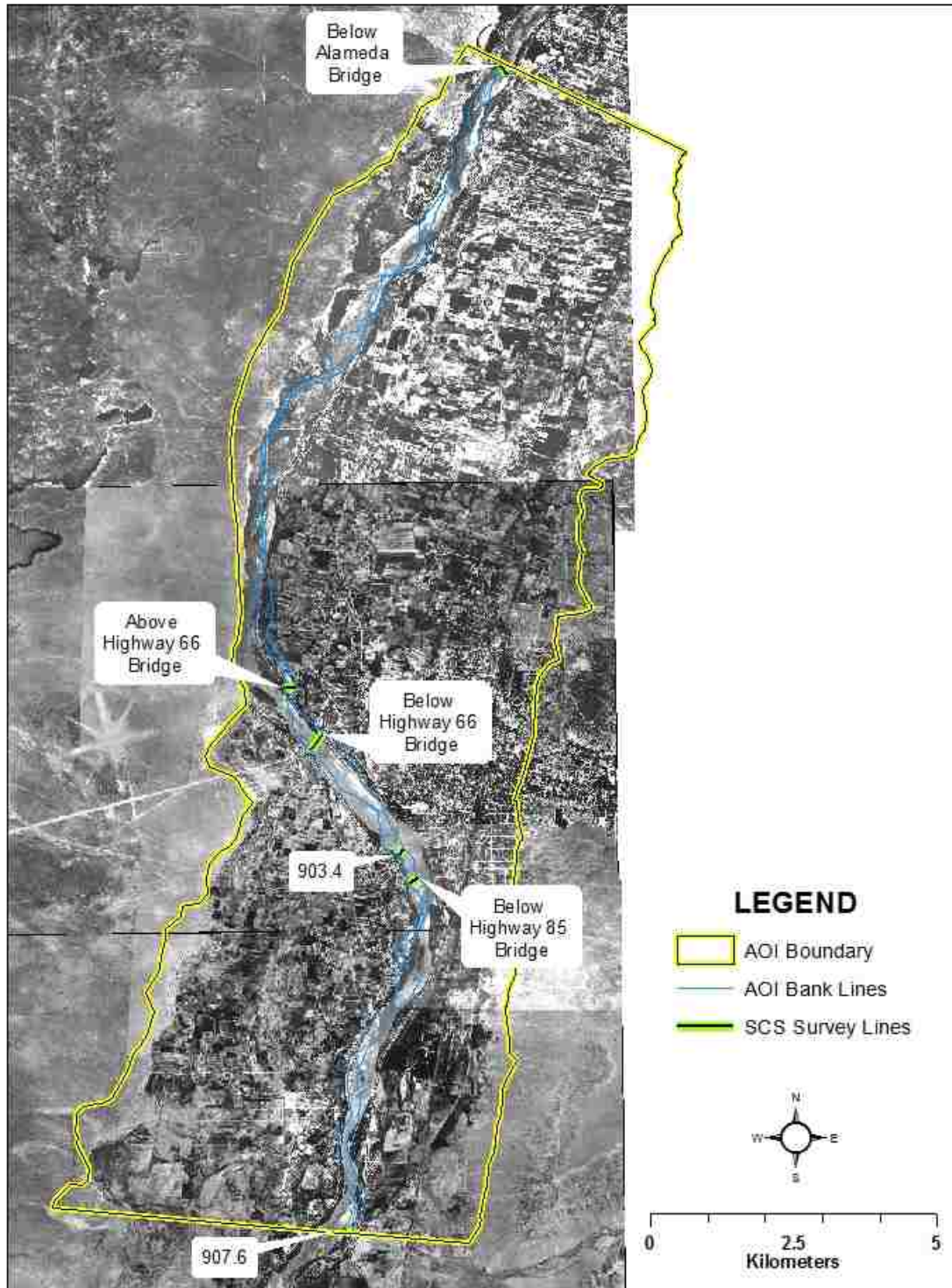


Figure 2: Estimated SCS survey line locations and Rio Grande bank lines shown within the boundary of the study reach AOI. Basemap is the 1935 aerial photography from USBR.

3.2 Current Data

In order to evaluate changes over time, an additional model was created to represent present day conditions. This model, referred to hereafter as the “modern model”, consists of a DEM that combines traditional survey data with data collected using Light Detection and Ranging (LiDAR) technology. LiDAR provides high resolution topographical data for the modern floodplain, including a 2010 LiDAR dataset and supplementary 2012 LiDAR elevation data at river restoration features. Floodplain topography was extracted from LiDAR, while channel bathymetry was built using 2014 channel survey data from USBR and a similar methodology to that of the reconstructed historical channel. As for modern land cover, vegetation classifications for the reach were obtained from a vegetation mapping effort led by multiple agencies from 2002 to 2004 as part of the Upper Rio Grande Water Operations Review and Environmental Impact Statement (URGWOPS). This includes a GIS shapefile consisting of varying polygons and an attribute table populated with modified Hink and Ohmart (1984) vegetation codes based on vegetation height and understory density. For this project, land cover classifications were converted to Manning’s n roughness values based on suggestions from a study done on the San Joaquin River (MEI, 2002b).

4 Geospatial Reconstruction Methods

4.1 Floodplain Topography

Using ArcGIS 10.1, a GIS software from Esri, the digitized maps were trimmed to include features only within the study reach. Because the maps were originally hand

drawn, many of the digitized lines were discontinuous. Therefore, lines of constant elevation were reconnected and dissolved into a single feature with the “Unsplit Line” tool, forming a set of contour lines. Elevation values marked on the topographic maps were assigned as elevation attributes to each contour line individually. Finally, contour lines were converted from 2D features to 3D features using the “Feature to 3D by Attribute” tool and setting elevation as the target attribute field. Figure 3 depicts the digitized maps within the study reach location with emphasis placed on the isolated contour lines and river bank lines.

4.2 Channel Characteristics

Channel bathymetry was reconstructed using the Hydrologic Engineering Center's River Analysis System (HEC-RAS), a hydraulic modeling software from the United States Army Corps of Engineers (USACE), and HEC-GeoRAS, an extension within ArcGIS. According to a 1914 soil survey of the Middle Rio Grande Valley, the channel banks of the historical Rio Grande averaged between 0.61 m (2 ft) and 0.76 m (2.5 ft) above the river bed and were rarely more than 0.61 m (2 ft) high (Soil, 1914). As this project is concerned with large flood flows, emphasis was placed on capturing general characteristics like channel width, channel depth, and streambed irregularity rather than identifying exact locations of historical features. This approach allowed for approximation of survey line locations.

Because the available SCS survey lines consist of station-elevation pairs that are not georeferenced, the data required placement and modification to be used as bathymetric data in reconstructing the historical channel. The objective here was to generate X-coordinates, Y-coordinates, and elevations (i.e., XYZ points) in order to build a 3D surface, or terrain. First, bank points were identified along the SCS survey lines so that each transect encompassed the channel only. The original survey data with delineated channels are plotted in Appendix B, along with a historical map showing locations of two survey lines within the study reach. Survey line locations were approximated and digitized in ArcGIS by using survey line names as a reference to location. For example, the "Below Highway 85 Bridge" survey line was located downstream of where Highway 85, present day New Mexico State Road 314, crosses the

Rio Grande, while the “903.4” survey line was located about 0.4 miles from milepost 903 along the Santa Fe Railway. Since the surveys are from 1936 and 1937, the 1935 aerial photographs also provided a means of estimating locations based on similar channel widths.

However, as previously mentioned, 1918 channel widths differ from 1935 channel widths. Therefore, the survey lines were scaled to fit the 1918 channel by multiplying stations by a width ratio:

$$\text{Width Ratio} = \frac{W_{\text{Transect}}}{W_{\text{SCS}}} \quad (1)$$

where:

W_{Transect} = width of 1918 channel at transect location

W_{SCS} = width of delineated channel from SCS survey line

A MATLAB code (See Appendix C) was developed to automate this process for all survey lines. This MATLAB code also calculated XY coordinates for station and elevation pairs based on right bank (X_R, Y_R) and left bank (X_L, Y_L) coordinates identified from ArcGIS at the approximated transect locations. Lastly, channel elevations in each survey line were adjusted by a fixed ΔZ to effectively set the transect into the 1918 channel. Ultimately, the MATLAB code generated a text file with XYZ points for each SCS survey line that had been transformed to fit the 1918 channel.

In order to format these transformed SCS survey lines into geometric data accepted by HEC-RAS, the XYZ points were incorporated into cross-section cutlines using HEC-GeoRAS. Cross-section cutlines were digitized at each of the SCS survey line locations and drawn across the extent of the floodplain to include the previously

identified right bank and left bank coordinates (Figure 4a and 4b). These cutlines were converted to 3D features using elevations from the floodplain and did not include channel bathymetry. So, the “Update Elevations” tool was used to replace the existing cutline elevations between channel bank points with the XYZ points (Figure 4c).

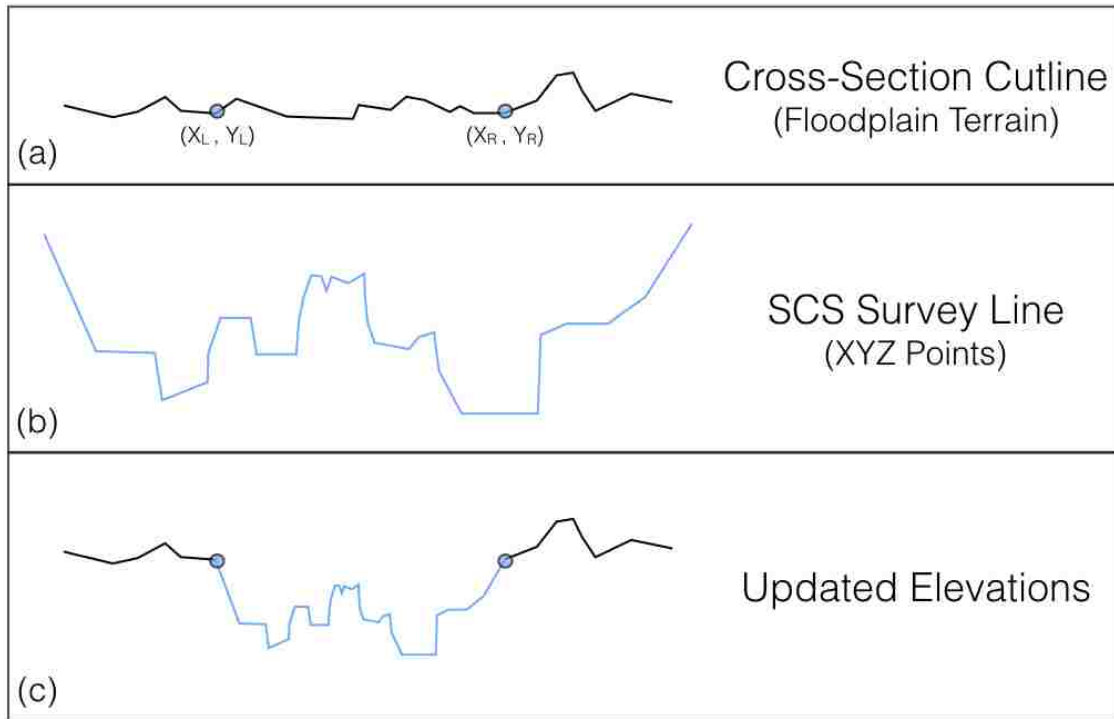


Figure 4: Schematic (i.e., not actual data) of the formatting process for HEC-RAS cross-section creation within GIS: (a) cutline digitized, bank points identified by coordinates, and elevations extracted from the floodplain terrain; (b) SCS channel survey line as XYZ points; (c) channel bathymetry merged with floodplain terrain between bank points.

After the updated geometry data was imported into HEC-RAS, cross-sections were manually trimmed closer to the bank lines and edited to remove any unnecessary points within the channel boundary. Due to the distant spacing of these constructed cross-sections, additional cross-sections were interpolated within HEC-RAS at a spacing of approximately 15.24 m (50 ft). Figure 5 provides a visual of how distant the untrimmed, constructed cross-sections were in comparison to the closely spaced

interpolated cross-sections, allowing for improved definition of channel bathymetry.

Interpolated geometry was exported from HEC-RAS as a spatial data file (SDF). However, file reformatting was needed in order to import the cross-sections into ArcGIS as a text file containing XYZ points for cross-section polylines. Another MATLAB code was written to automate the formatting process. Within ArcGIS, the “Feature Vertices to Points” tool converted the interpolated cross-sections back to XYZ points as opposed to polylines. Finally, these points were clipped to within the bank lines to only represent channel bathymetry.

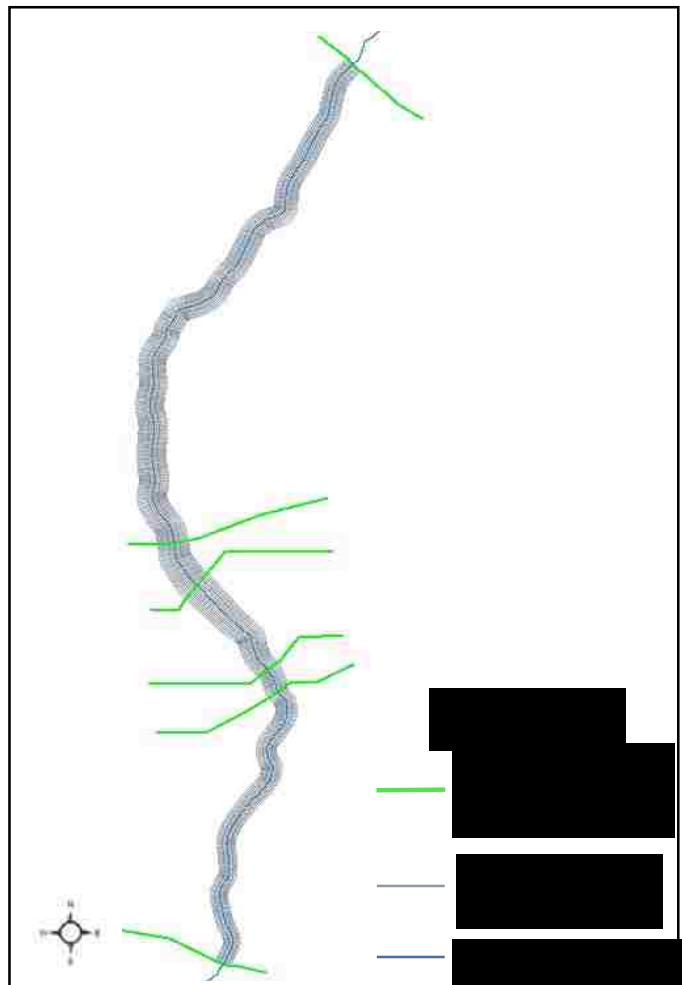


Figure 5: RAS Mapper view of the study reach AOI showing cross-sections imported from GIS at each SCS survey line location and cross-sections interpolated using HEC-RAS.

4.3 Land Cover

In terms of land cover, the topographic map set describes not only vegetation types, but soil classifications and land uses as well. Examples of vegetation types depicted and labeled on the 1918 maps are shown in Table 2. Table 3 includes other features displayed on the maps, including soil classifications, land use types, and mile post markings along the railroad that correspond with the SCS survey lines.

Table 2: Examples of vegetation types shown on the 1918 topo maps.

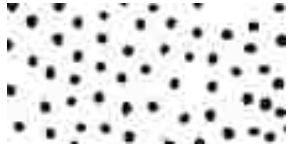
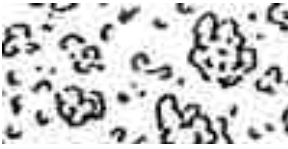



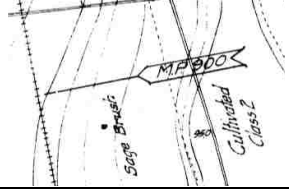
Symbol			
Label	<i>Shrub</i>	<i>Timber</i>	<i>Timber & Brush</i>

Table 3: Examples of soil types, land uses, and markers shown on the 1918 topo maps.

Symbol			
Description	Soil Classification	Land Use Type	Mile Post
Label	<i>Sand Bar</i>	<i>Cultivated Area Class 1</i>	<i>M.P. 900</i>

Bloodgood (1930) described seven categories of land cover types that correspond with the 1918 maps: cultivated class 1, cultivated class 2, alkali and salt grass, swamp, timber, river or river wash, and other. Cultivated classes indicated the extent of the effects of a rising water table, where class 1 showed no visible effects on crop growth and class 2 showed evidence of crop injury or high alkali levels due to a

high water table. While only sporadically visible on the 1918 maps, diversification of crops following the introduction of the Santa Fe Railway also brought about more intensive agriculture like fruit orchards, particularly apple, throughout the valley (Soil, 1914).

In terms of land not utilized for farming, Bloodgood (1930) described alkali areas overgrown with salt grass and timber areas overgrown with cottonwood, willows, and thorn bushes. These categories are consistent with observations from Van Cleave (1935) claiming that salt grass was most prevalent in areas of high alkali concentrations. Cottonwood forests, commonly located along the river corridor, likely had little understory, as periodic flooding flushed out herbaceous vegetation and canopy shading discouraged ground cover growth (Van Cleave, 1935). This is an important distinction between areas classified as either timber or cottonwood, especially in terms of estimating vegetative roughness.

Swamps, or marshy areas with exposed groundwater, were resultant of supplemental irrigation water from agricultural ditches as well as the river's perched elevation from heavy silt deposition (Bloodgood, 1930; Van Cleave, 1935). Vegetation types in these marshy areas were similar to those found in a shallow lake environment: algae, cattail, sedges, rush, watercress, and buttercup (Van Cleave, 1935). Meadow land, commonly used for grazing, consisted of salt grass, sedges, rush, and lizard tail (Bloodgood, 1930; Van Cleave, 1935). River or river wash included not only the main channel, but also side channels labeled on the 1918 maps as sloughs that were washed

during high flow, had sand and gravel beds, and lacked vegetation (Bloodgood, 1930). All other areas included, but were not limited to, town land, ditches, and sand dunes.

Land cover polygons were digitized in ArcGIS to represent the spatial distribution of vegetation type. Each polygon was assigned a land cover or land use attribute based on demarcations from the 1918 maps. To ensure the entire model extent contained a classification (i.e., no gaps), a polygon was drawn over the entire reach and assigned the attribute of unclassified. Using the “Erase” tool, the existing land cover polygons were removed so that only potential gaps remained and these remaining unclassified areas were appended to the land cover shapefile using the “Append” tool. To prepare this final land cover shapefile for model input, multipart features were removed with the “Dissolve” tool.

Because hydrodynamic modeling requires roughness as a quantitative resistance parameter as opposed to a qualitative vegetation type, land cover classifications were each related to a Manning’s roughness coefficient: Manning’s n . These relations were based on aforementioned descriptions from Bloodgood (1930), Van Cleave (1935), and suggestions from various reference tables, including Chow (1958) and a study done on the San Joaquin River (MEI, 2002b). Manning’s roughness values from the conversion table (Table 4), were appended to the land cover table in ArcGIS using a table join with the common land cover attribute. Open water, referring to both the main channel and sloughs, has a Manning’s n value of 0.025, which is consistent with values ranging from 0.02 to 0.026 assigned for the main channel of the Rio Grande in reaches throughout the Middle Rio Grande (Leon et al., 2009; Novak, 2006). As expected, Manning’s n for

the 1918 channel is less than the value chosen for the present day channel, 0.032, because over time, an increasing median grain size in the channel bed has increased bed roughness (Novak, 2006).

Table 4: Land cover classifications and corresponding Manning's n values.

Land Cover	Manning's n	Land Cover	Manning's n
Alkali	0.030	Open Water	0.025
Brush	0.100	Orchard	0.035
Butte	0.045	Sage Brush	0.050
Cottonwood	0.060	Sand Bar	0.032
Cultivated Class 1	0.040	Sand Dunes	0.032
Cultivated Class 2	0.030	Sand and Sage Brush	0.050
Grass	0.030	Timber	0.100
Marsh	0.028	Unclassified	0.050
Meadow	0.035	Urban	0.038

5 Hydrodynamic Modeling

Two-dimensional (2D) hydrodynamic modeling was selected as a means of quantifying the effects of historical river modifications on inundation patterns.

Hydrodynamic modeling was performed on both historic and current conditions based on historical flood scenarios. Finally, the model results were analyzed using inundated area and displayed using floodplain inundation mapping. These inundation maps aid in visualizing the effects of historical river engineering, particularly how channelization has influenced channel-floodplain connectivity (Hohensinner et al., 2004).

5.1 Model Selection and Development

The historic, or retro-model, and modern model were built using D-Flow Flexible Mesh (D-Flow FM), an open source 2D hydrodynamic model from Deltares in the Netherlands (Deltares, 2014). Model input files prepared within GIS were loaded into D-Flow FM where various tools were used to generate the unstructured mesh, or network, on which computations were executed. The curvilinear mesh combined rectangular grid cells in the main channel with triangular grid cells on the floodplain to capture more complex topography. A significant advantage to using D-Flow FM is the ability to create a multi-resolution mesh, with low resolution in areas of lesser interest and high resolution in areas of interest. For comparison purposes, the retro-model and modern model meshes were of consistent resolutions.

5.2 Mesh Refinement and Parallelization

Enhancement of the mesh is critical to model accuracy by ensuring the network is orthogonal and smooth. An ideal refined mesh would have 90° angles between flowlinks and netlinks along with adjacent cells that have equal areas (Deltares, 2014). Another significant advantage to D-Flow FM is the capability for parallelization. Parallelization reduces model run-time and requires partitioning of the network and input file known as the Master Definition Unstructured file (MDU-file). The mesh was partitioned by creating partitioning polygons through the D-Flow FM GUI, while the MDU-file was partitioned from the command line. The number of partitions depends on the number of nodes available for use on the supercomputer. All partitioned models for

this project ran on a Linux-based supercomputer at the Center for Advanced Research and Computing (CARC) at the University of New Mexico (UNM).

5.3 Flow Conditions

Both models were run under a range of steady-state flow conditions: 142 m³/s (5,000 cfs), 283 m³/s (10,000 cfs), 425 m³/s (15,000 cfs), and 566 m³/s (20,000 cfs). The highest flow was chosen to represent the last large flood of 1942 with a daily mean discharge peaking at approximately 566 m³/s as measured from the Rio Grande at the Albuquerque gage (See Appendix D). According to Swanson et al. (2011), annual peak floods in Albuquerque averaged about 420 m³/s between 1895 and 1918 with eight floods reaching flows greater than 550 m³/s from 1884 to 1920. This account of hydrologic data further verified the modeled discharges as an accurate reflection of historical flood conditions for the time period of interest.

6 Results

6.1 Geospatial Inputs

Geospatial reconstruction of the historical Middle Rio Grande resulted in two primary inputs necessary for building the retro-model: the retro-DEM and distribution of roughness. Figure 6 maps the land cover classification types present throughout the AOI and is testament to the great variation of roughness in the historical Albuquerque reach. Areas of higher elevation were associated with high roughness vegetation such as sage brush, while the majority of the floodplain was covered with farmland and the channel was directly bordered by sand bars and patches of timber.

The retro-DEM in Figure 7 ultimately represents the historical surface of the AOI, with detailed sub-areas shown in Figure 8. The DEM was generated by first creating a triangulated irregular network (TIN) surface model with the “Create TIN” tool using a polygon mask as a soft clip for the TIN boundary, contour lines and channel banks as hard break lines for floodplain topography, and cross-section points as mass points for channel bathymetry. This TIN was then converted to a raster with a 1 m (3.28 ft) resolution using the “TIN to Raster” tool.

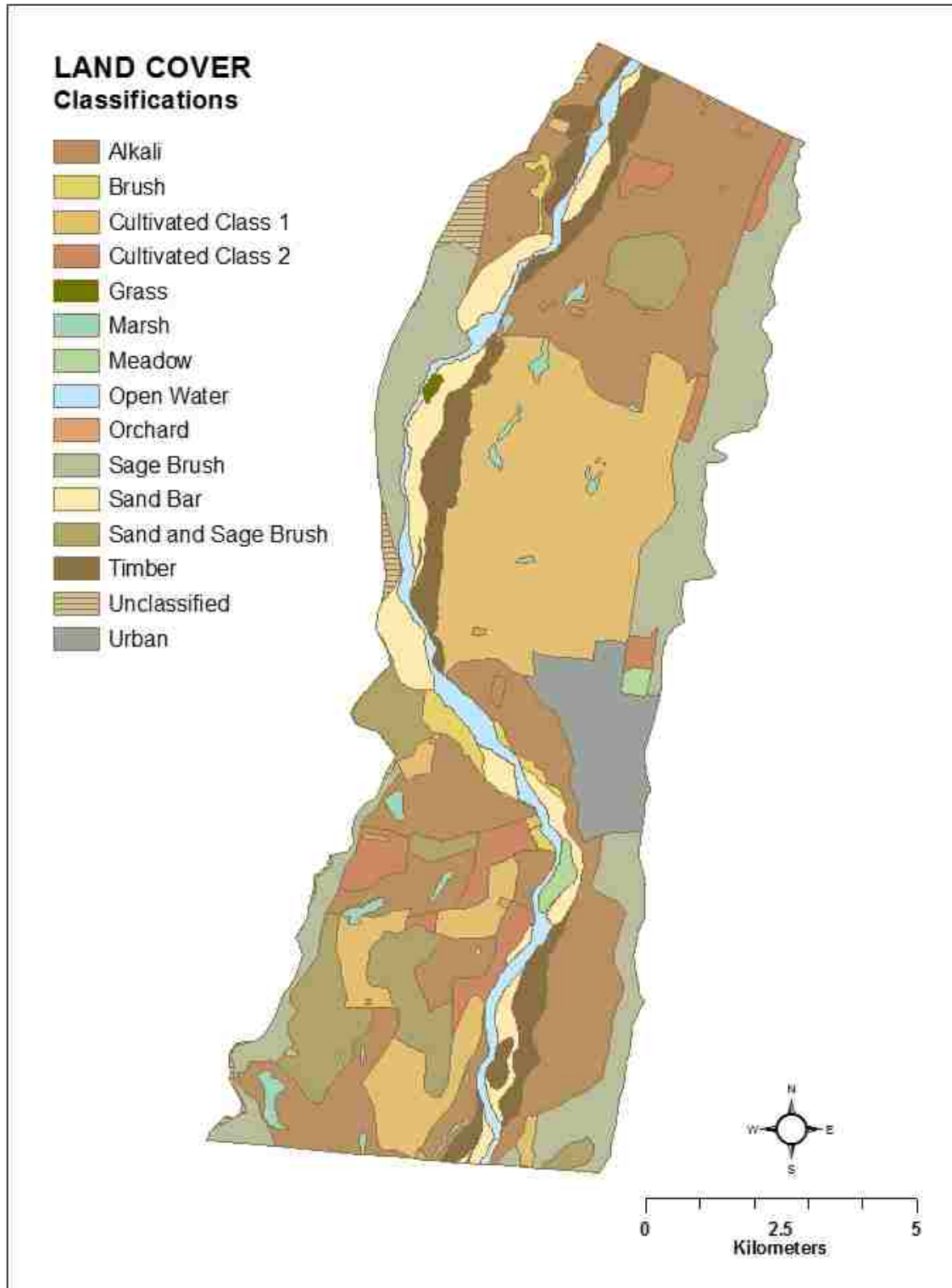


Figure 6: Land cover classifications within the AOI of the study reach.

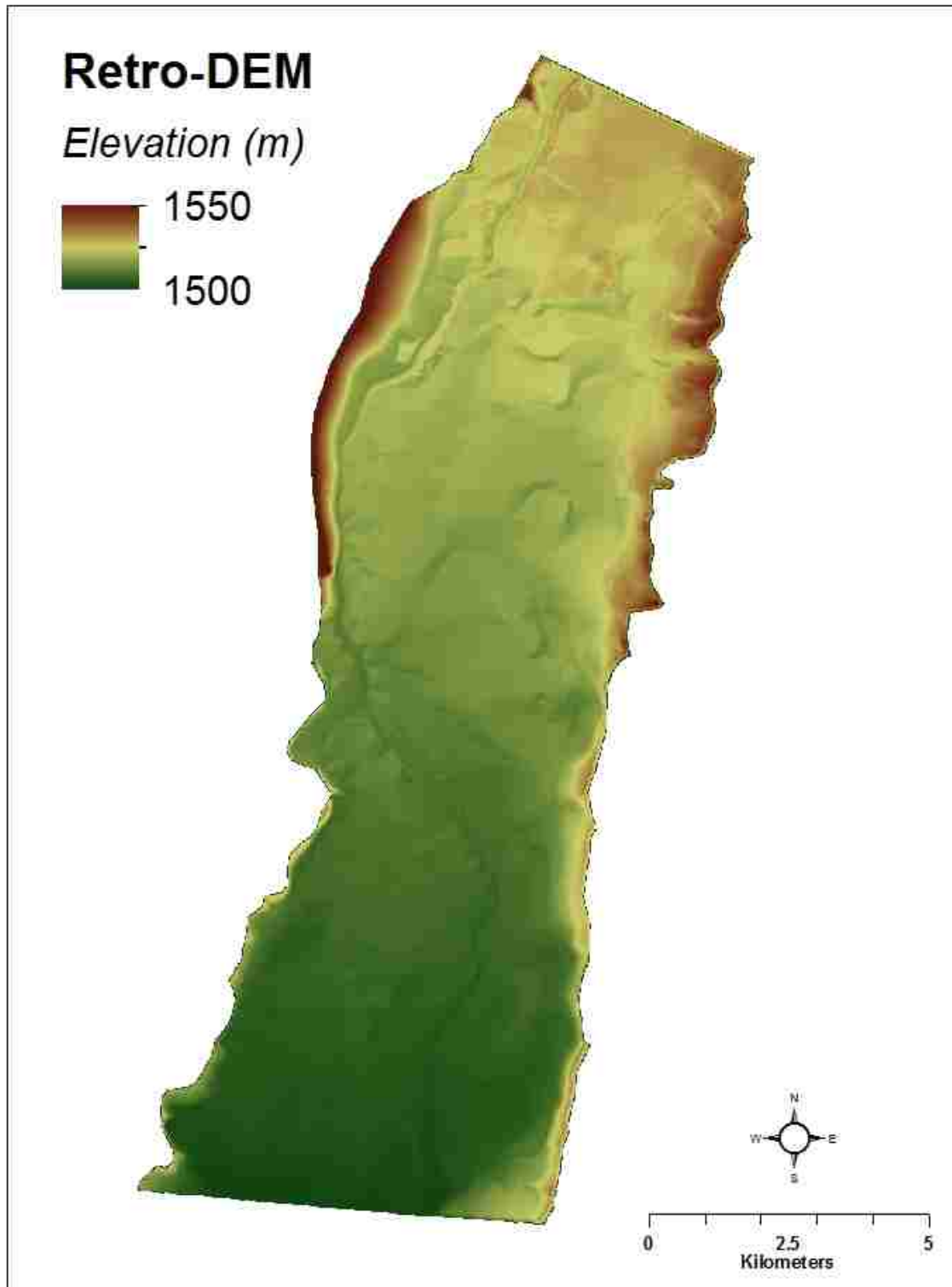


Figure 7: Retro-DEM displayed with hillshade.

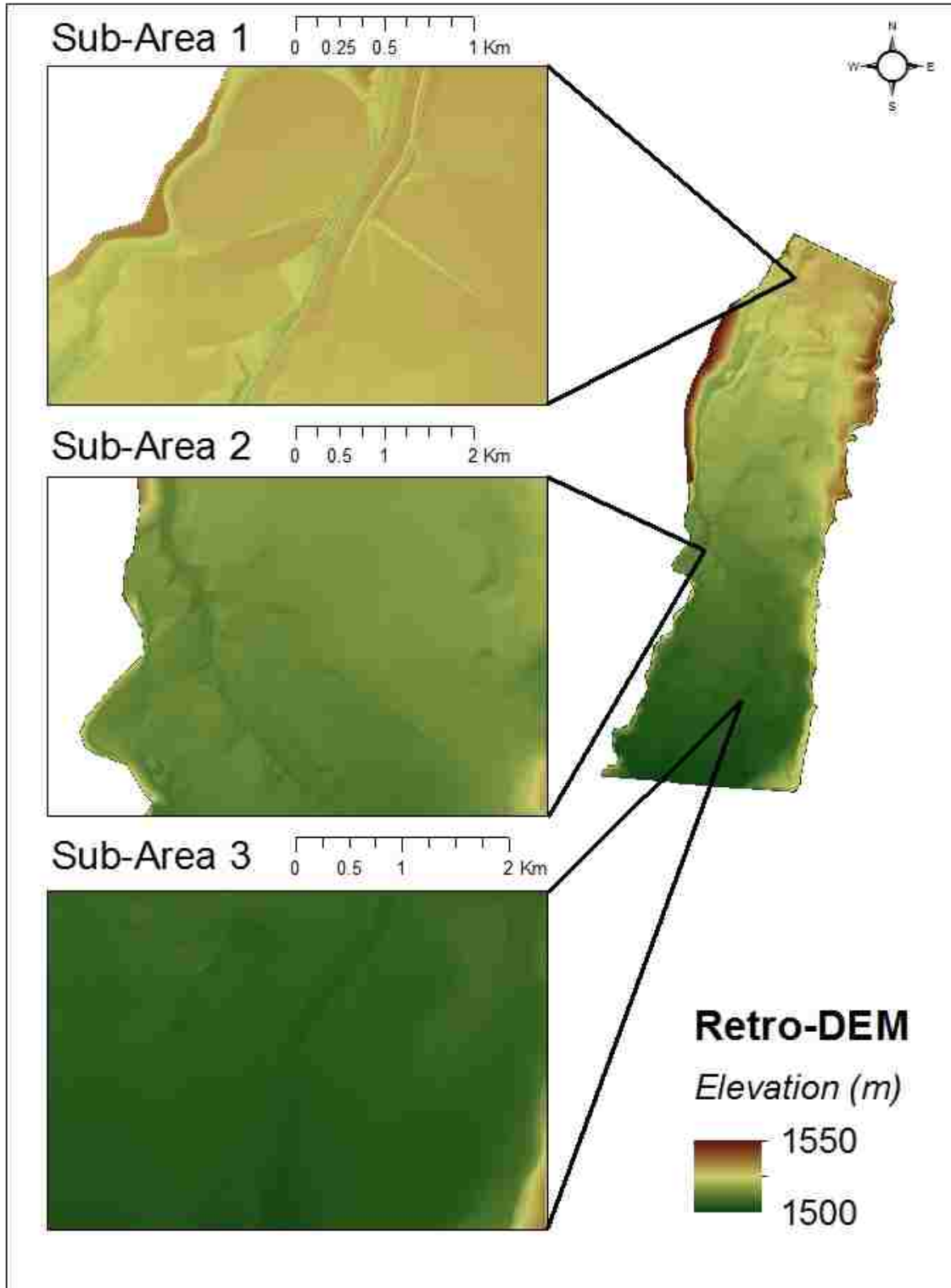


Figure 8: Expanded view of three sub-areas showing the retro-DEM in greater detail.

6.2 Inundated Area and Inundation Mapping

Model results were evaluated based on inundation to capture changes in lateral connectivity and flooding extent. In order to represent inundation both visually as well as quantitatively, water depth rasters were created using GIS. Model element data, including X-coordinates, Y-coordinates, and depth values, were extracted from the output from D-Flow FM, converted to feature points in GIS, and used to create a TIN. The TIN was converted to a raster with a conditional tool to remove all depth values less than or equal to zero. Boundary errors producing unrealistic water depths were eliminated by removing sections of raster values at the upstream and downstream boundaries.

Inundated area was calculated by multiplying the number of inundated raster cells by the cell area, 9 m². As shown in Table 5, inundated area was considerably greater historically than for modern conditions. In fact, over the range of flows, the amount of inundated area was reduced by an average of 81.5%.

Table 5: Comparison of inundated area for the historic and modern models under four flow conditions.

Flow Condition	Historic Model Inundated Area (km²)	Modern Model Inundated Area (km²)	% Reduction of Inundated Area
142 m³/s (5,000 cfs)	37.6	7.3	81
283 m³/s (10,000 cfs)	49.9	10.1	80
425 m³/s (15,000 cfs)	58.8	10.5	82
566 m³/s (20,000 cfs)	63.7	10.7	83

For further analysis, inundated area was differentiated as either channel inundation or floodplain inundation. The percentages of inundation occurring in the floodplain versus in the channel for each modeled scenario are compared in Table 6. Inundation maps were also generated for both 1918 historic conditions (Figures 9-12) and circa 2010 modern conditions (Figures 13-16) for each of the four specified flows. These maps visually support the finding that historically, across all modeled flow conditions, over 80% of inundation occurred in the floodplain. As for modern conditions, the majority of inundation remains in the channel at lower flows, while at higher flows inundation is split almost evenly between the channel and floodplain. This significant departure from historical inundation patterns suggests an overall loss of river-floodplain connectivity.

Table 6: Comparison of percent inundation located in the channel versus the floodplain for the historic and modern models at each flow condition.

Flow Condition	Model	% Channel	% Floodplain
142 m³/s (5,000 cfs)	Historic	19.0	81.0
	Modern	72.9	27.1
283 m³/s (10,000 cfs)	Historic	14.6	85.4
	Modern	52.4	47.6
425 m³/s (15,000 cfs)	Historic	12.5	87.5
	Modern	50.7	49.3
566 m³/s (20,000 cfs)	Historic	11.5	88.5
	Modern	49.7	50.3

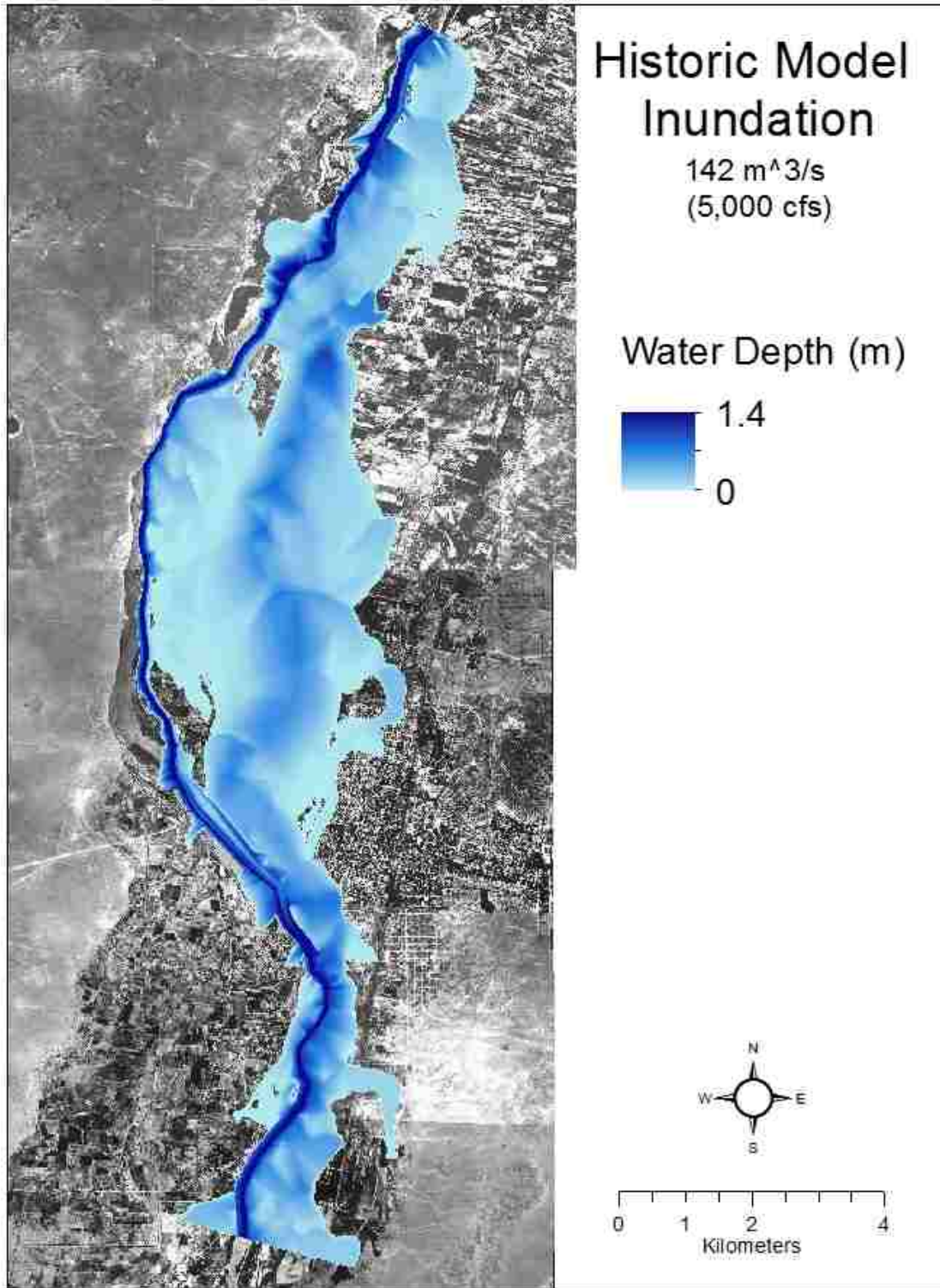


Figure 9: Inundation map for historic conditions at a flow of 142 m³/s (5,000 cfs).

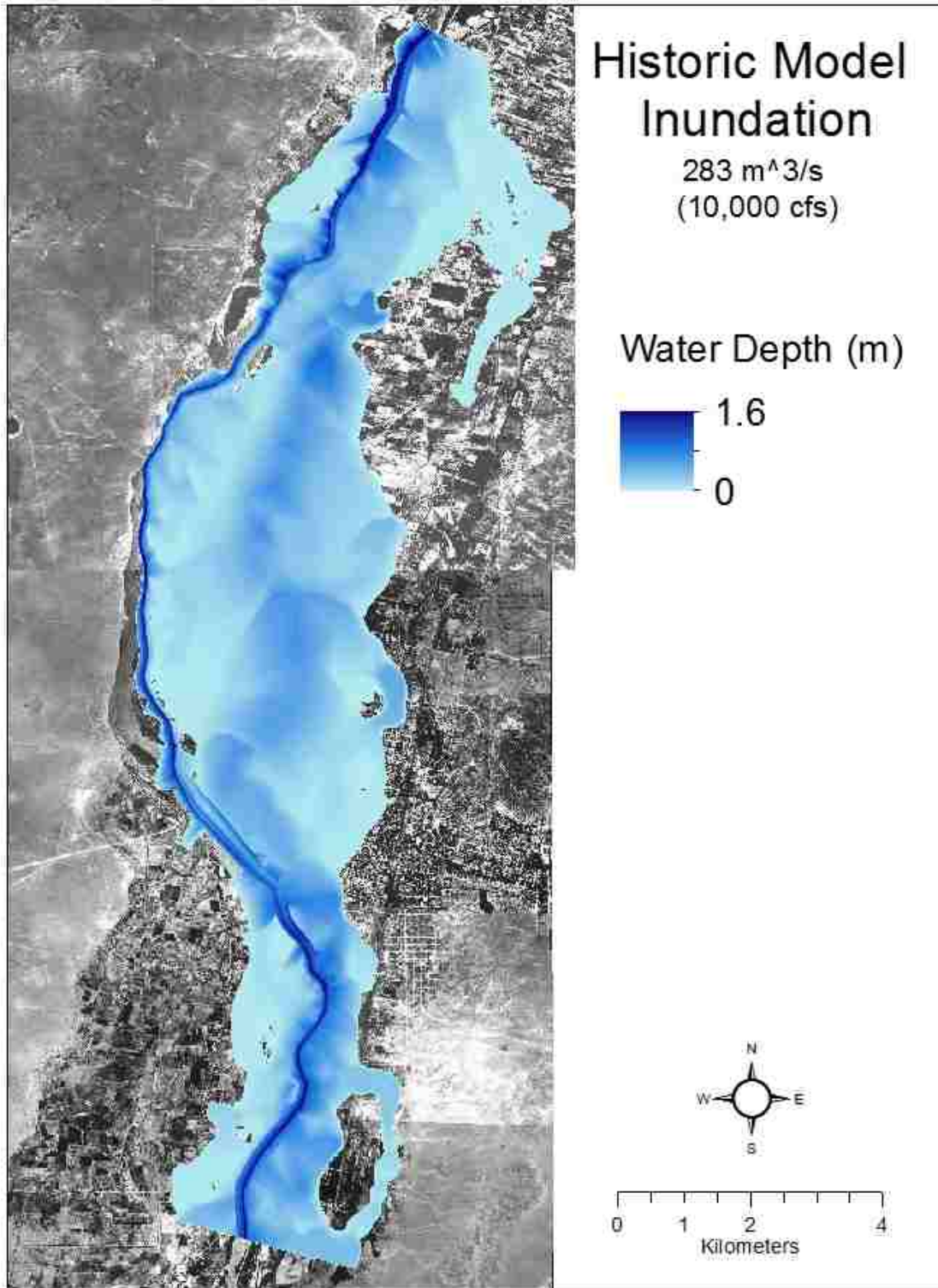


Figure 10: Inundation map for historic conditions at a flow of 283 m³/s (10,000 cfs).

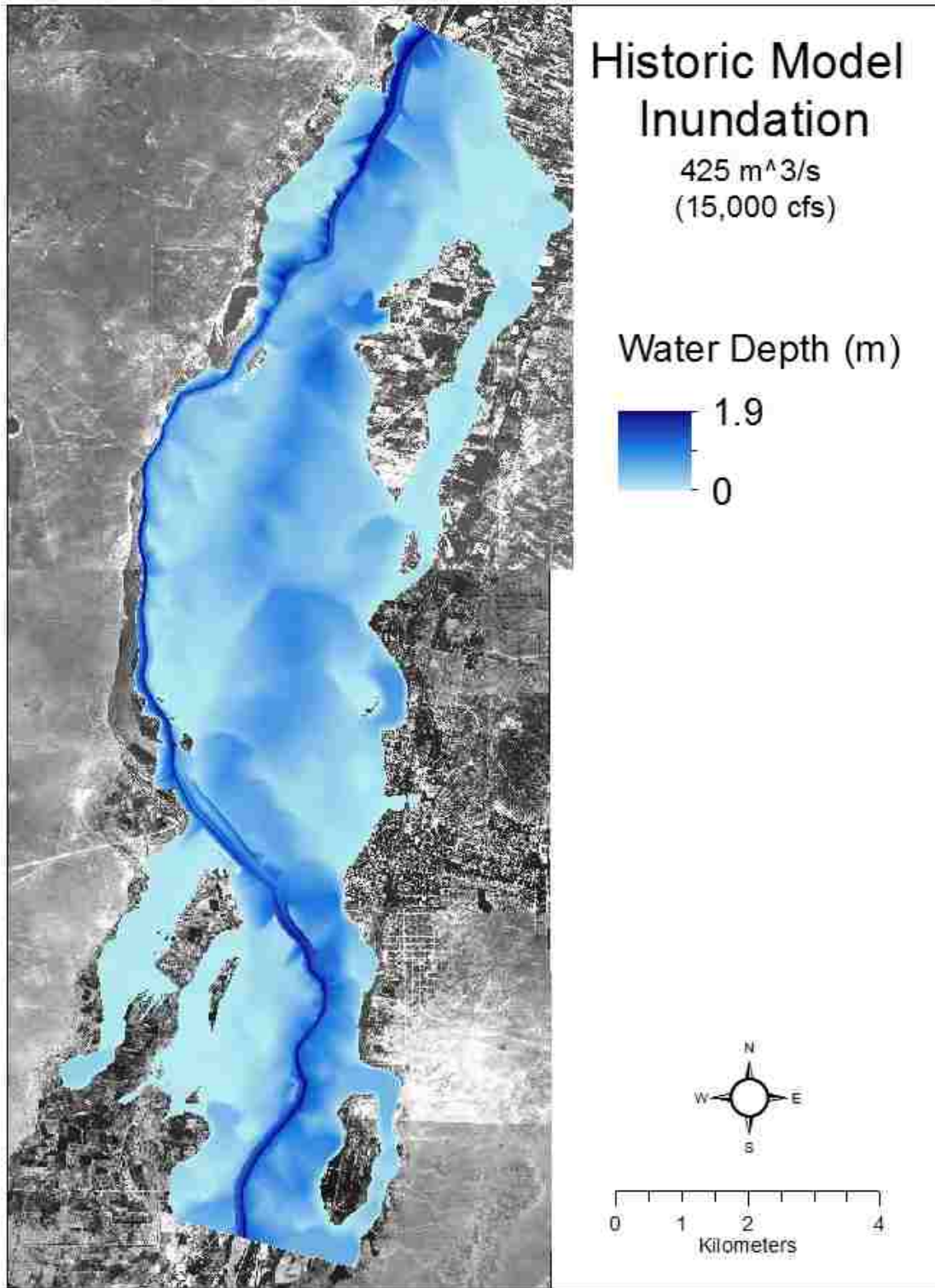


Figure 11: Inundation map for historic conditions at a flow of 425 m³/s (15,000 cfs).

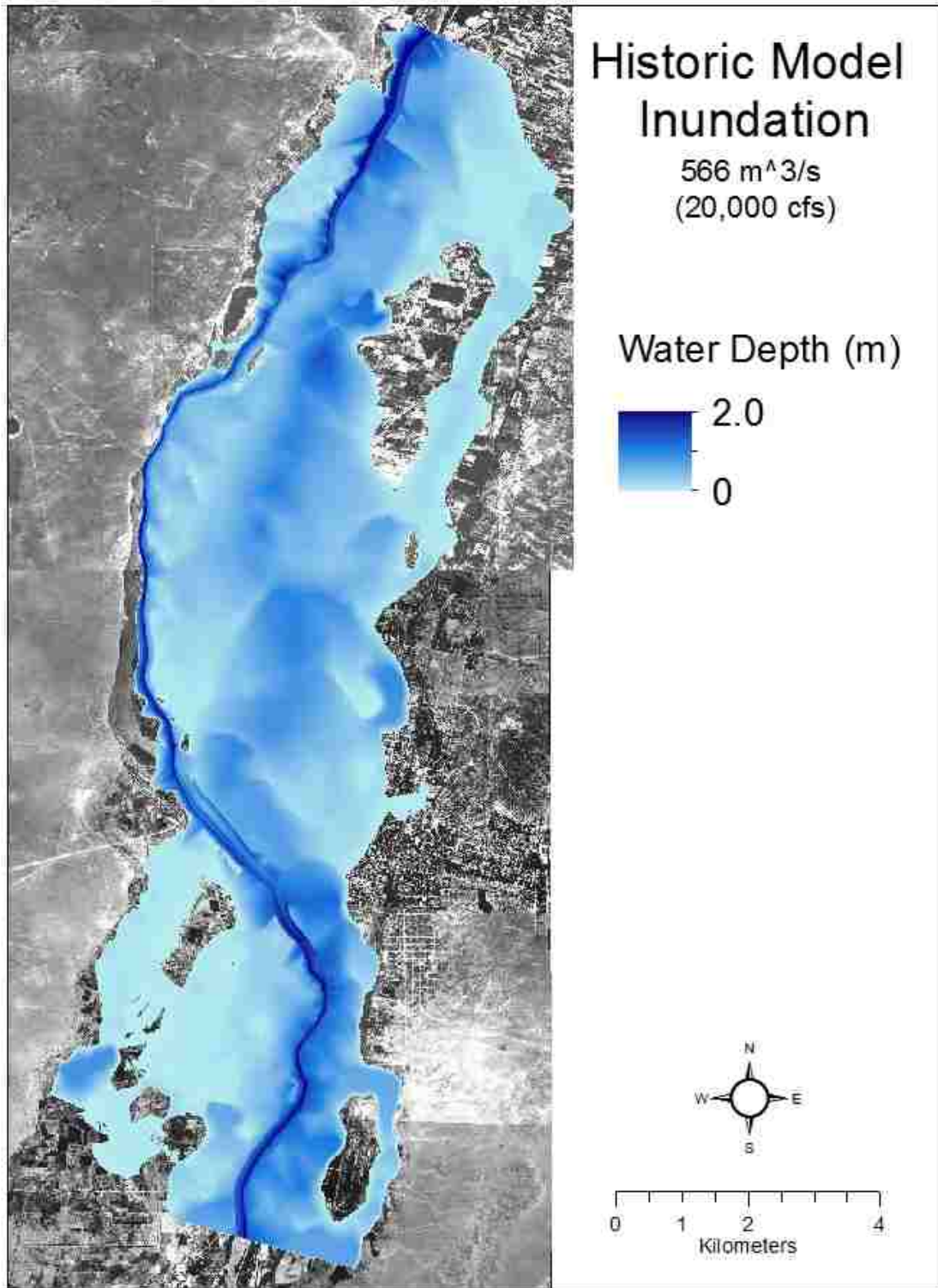


Figure 12: Inundation map for historic conditions at a flow of 566 m³/s (20,000 cfs).

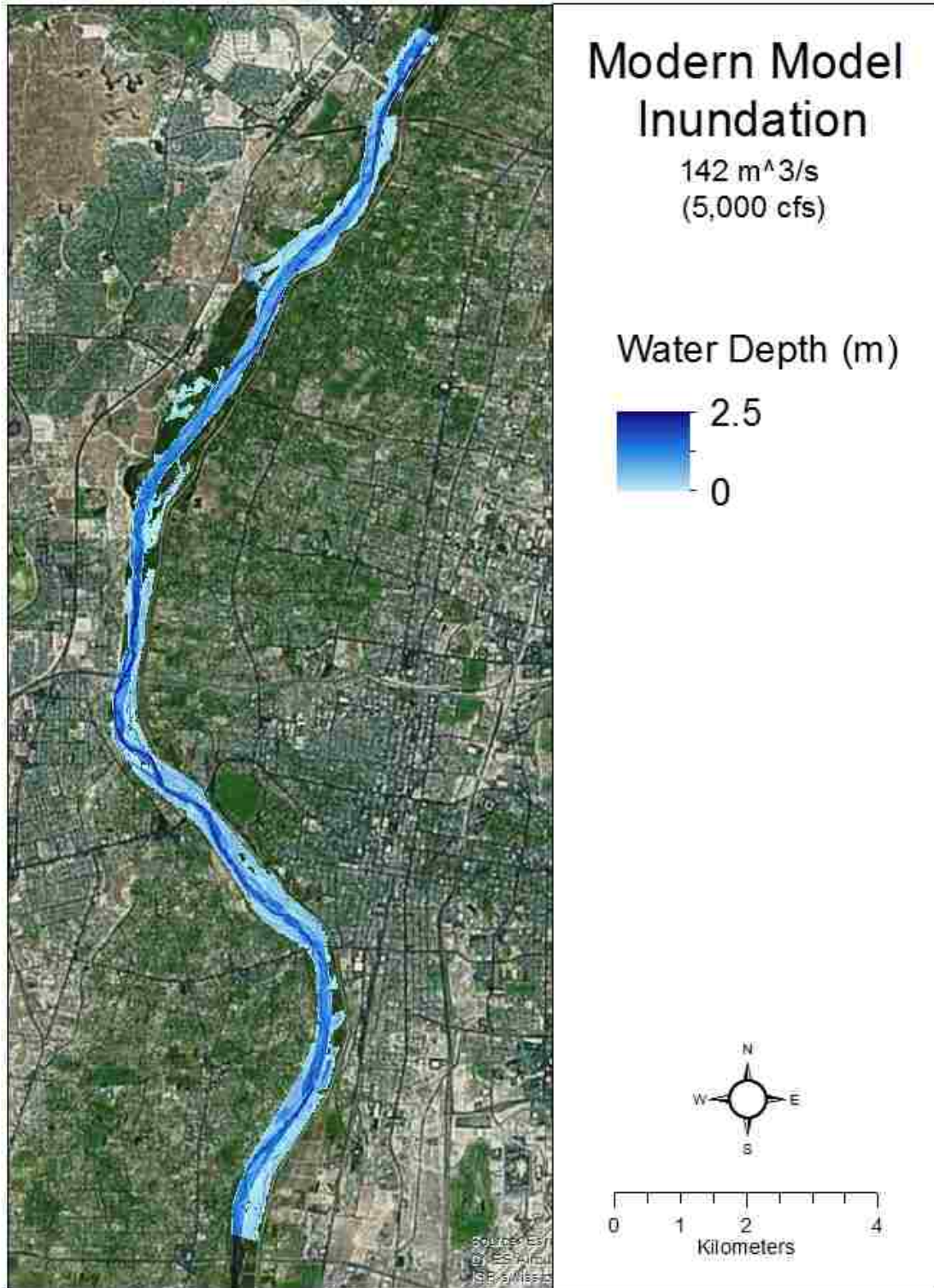


Figure 13: Inundation map for modern conditions at a flow of 142 m³/s (5,000 cfs).

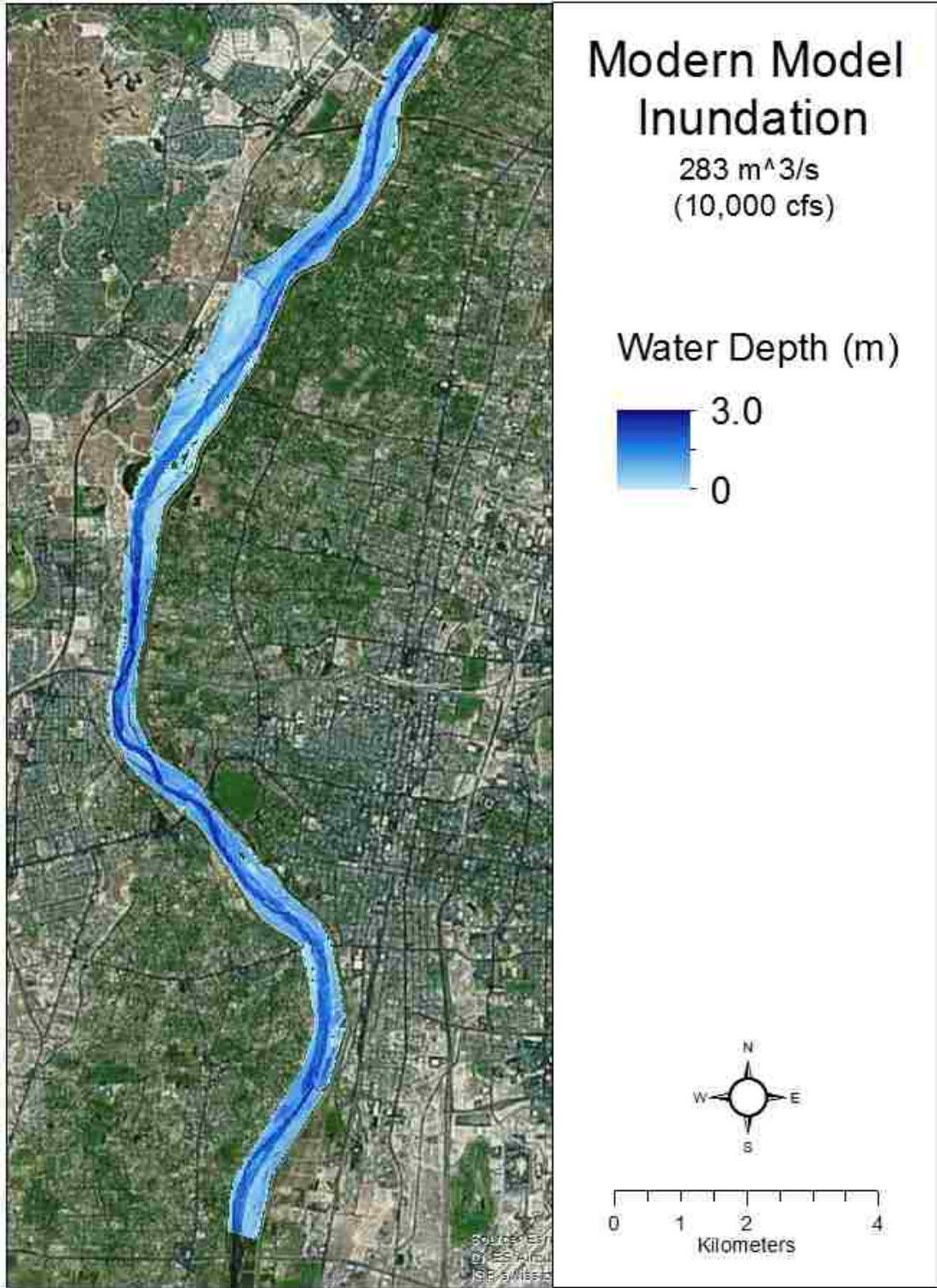


Figure 14: Inundation map for modern conditions at a flow of 283 m³/s (10,000 cfs).

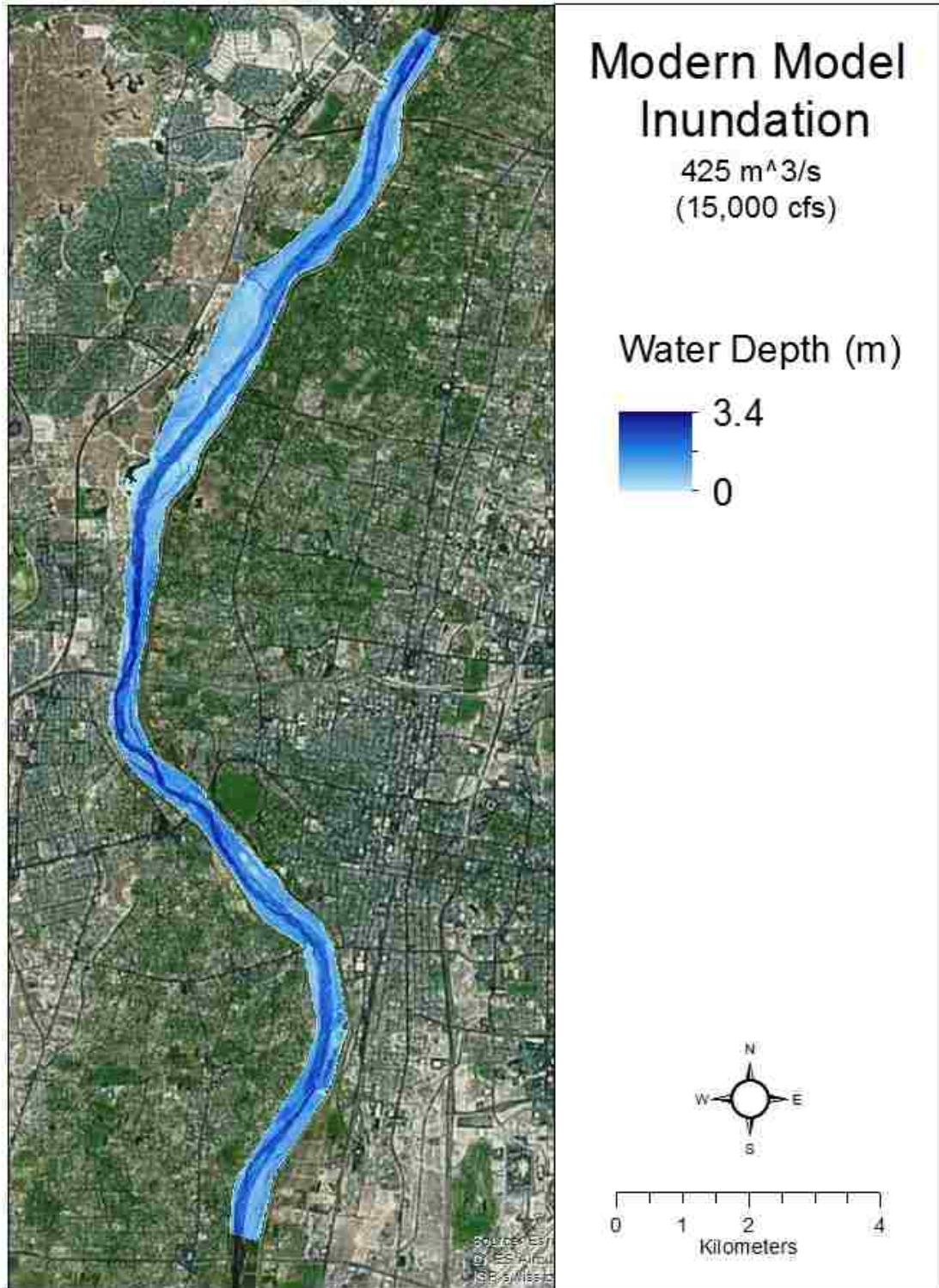


Figure 15: Inundation map for modern conditions at a flow of 425 m³/s (15,000 cfs).

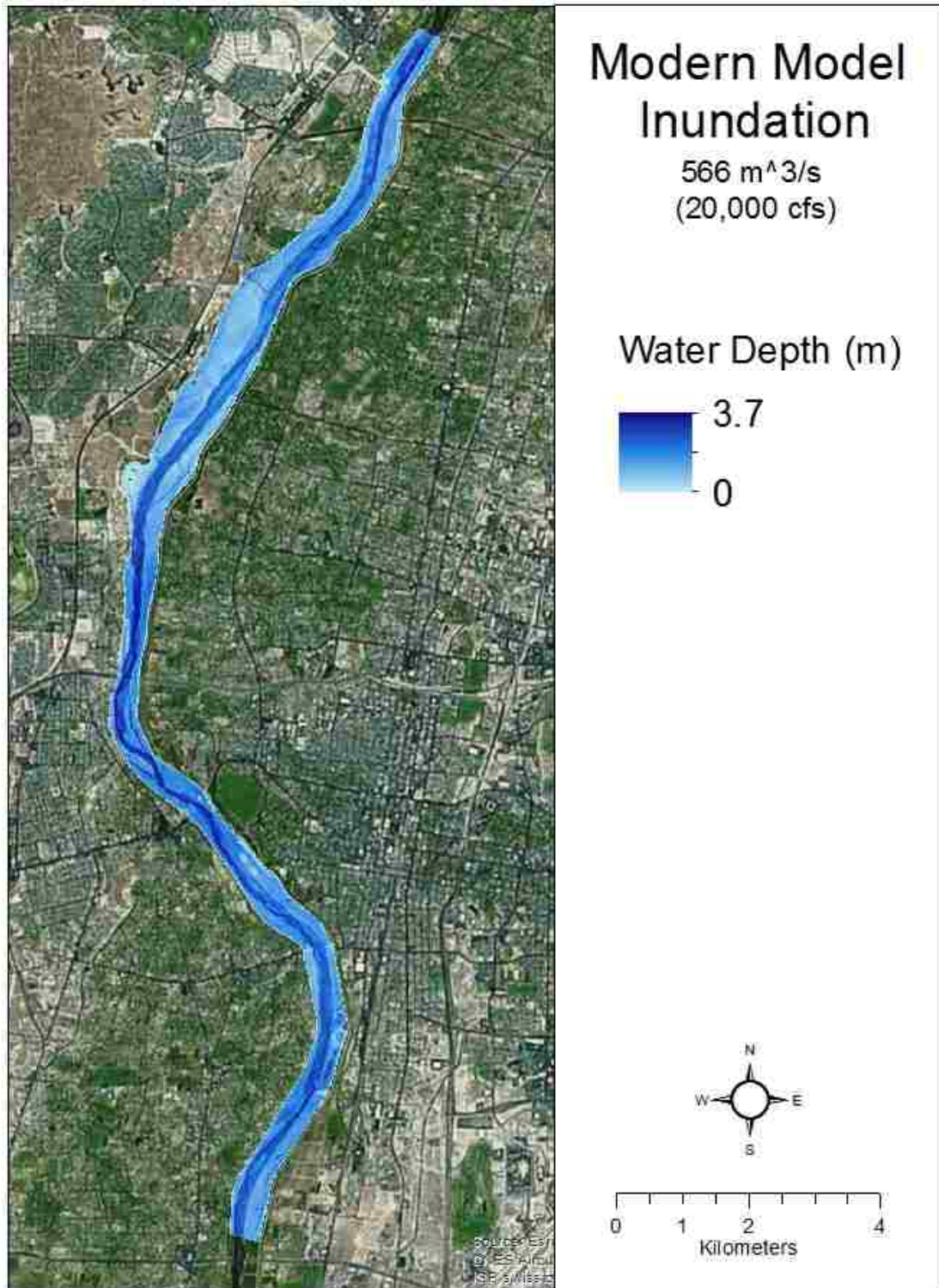


Figure 16: Inundation map for modern conditions at a flow of 566 m³/s (20,000 cfs).

6.3 Velocity Relative Frequency Histograms

Relative frequency histograms (Figures 17-20) were generated for the distribution of velocities across equal intervals, with velocity ranging from 0.0 to 2.8 m/s. The histograms represent changes in the magnitude and distribution of velocities between the historic and modern models. These changes are influenced by parameters such as floodplain roughness and channel capacity. Changing velocities should be taken into account by managers and planners due to its potential impact on the movement of flood waves, levees, and floodplain infrastructure.

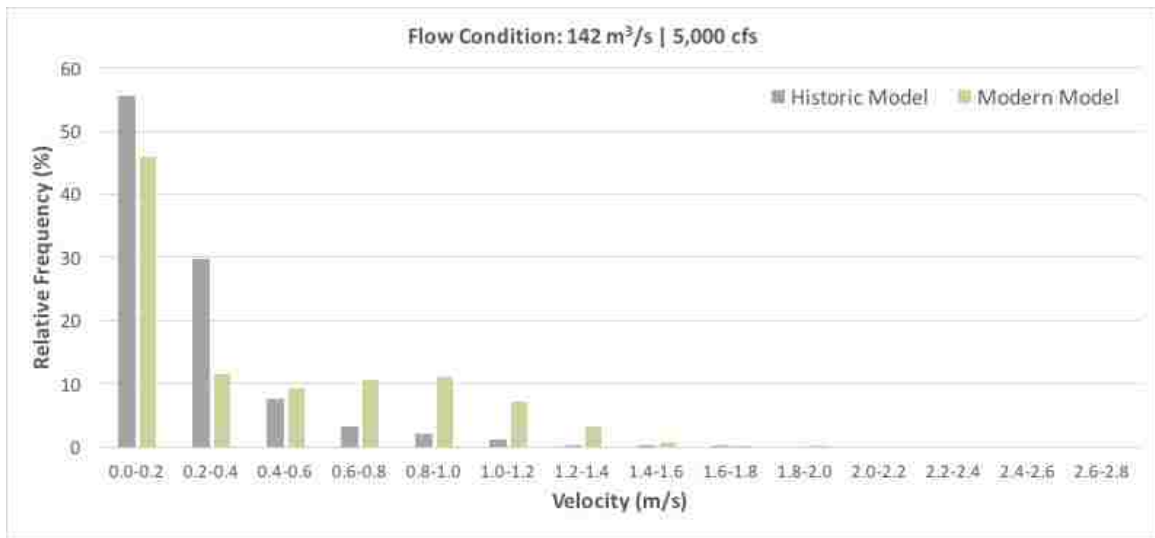


Figure 17: Distribution of velocities for the historic and modern models at a flow of 142 m³/s (5,000 cfs).

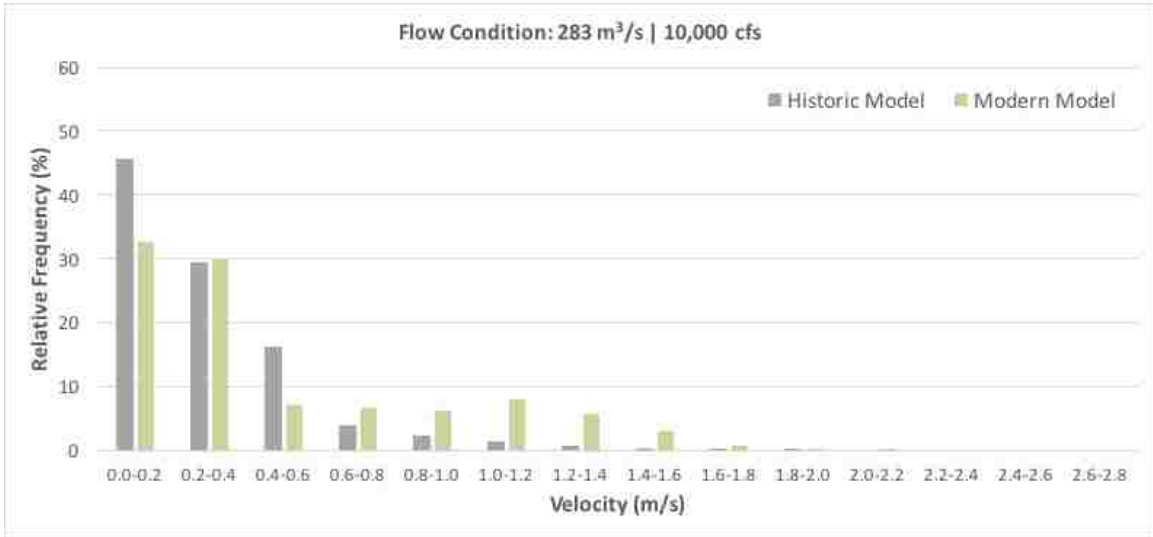


Figure 18: Distribution of velocities for the historic and modern models at a flow of 283 m³/s (10,000 cfs).

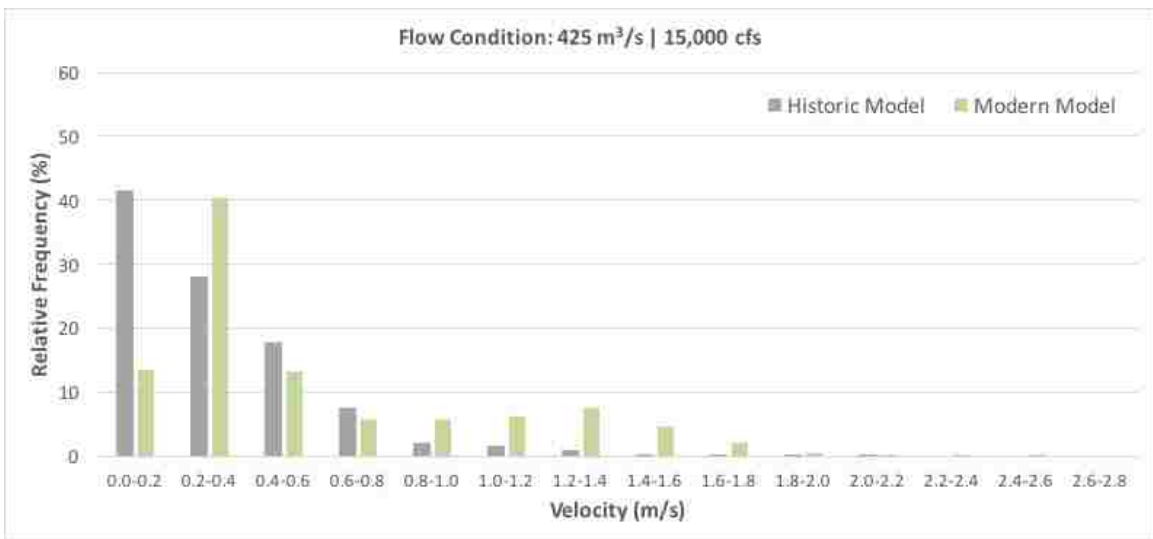


Figure 19: Distribution of velocities for the historic and modern models at a flow of 425 m³/s (15,000 cfs).

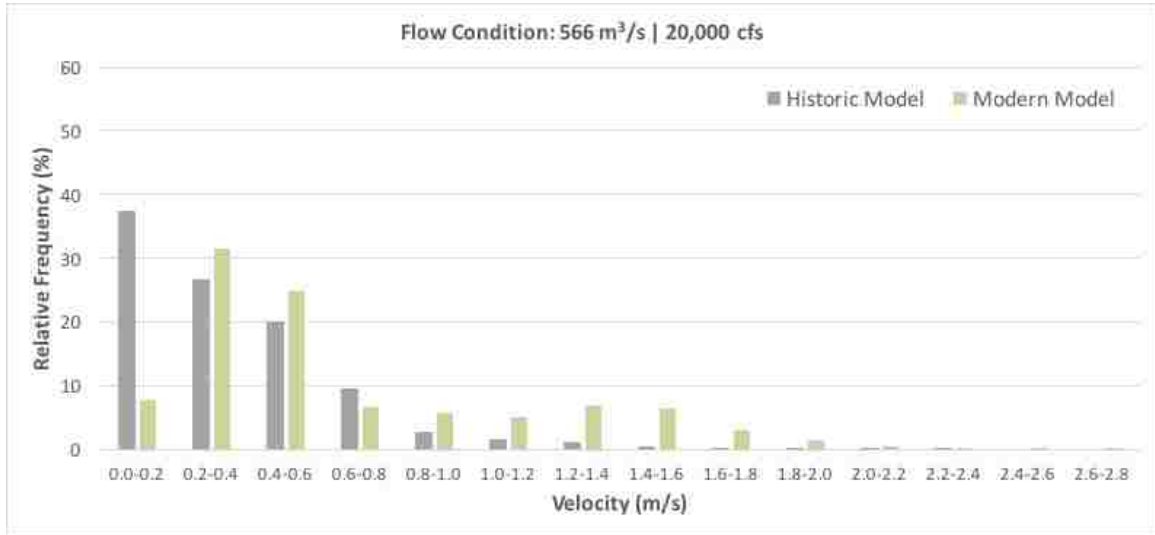


Figure 20: Distribution of velocities for the historic and modern models at a flow of 566 m³/s (20,000 cfs).

7 Discussion

Ultimately, this paper presents a holistic method for reconstructing the Albuquerque reach of the Middle Rio Grande, pre-MRGCD. The proposed method relies on the availability of a combination of historical sources, including maps, reports, and photos. Reconstructing and analyzing geospatial changes over time increases our understanding of interactions at the human-environment interface while also allowing us to make informed predictions of future changes (Yang et al., 2014). However, dealing with historical data presents numerous challenges related to inconsistent or insufficient scaling, formatting, and resolution. While this produces a level of uncertainty that would be unacceptable for design, for the purpose of the objectives in this paper, the knowledge gained provides an acceptable base condition necessary for comparing historic and current conditions. It is important to note that the models are uncalibrated because of the lack of historical data that would be needed for calibration. However, if

actual inundation data was available from around 1918, the models would be calibrated by adjustment of Manning's n roughness values until modeled water surface elevations closely matched measured data.

Even at the lowest modeled flow, there is a considerable amount of inundation in the historic condition, especially along areas of the floodplain that were known to be marshy. This excessive inundation can be explained in recognizing that the historic model does not account for makeshift flood control infrastructure within the Middle Rio Grande Valley. Various historical records (e.g., Soil, 1914; Van Cleave, 1935) confirm that at the time, levees or dikes were built to prevent both river migration and this extent of flooding from occurring. Consequently, the retro-model is considered the most unconstrained historic condition and identifies most closely with the river's natural response to flooding. Modern conditions, on the other hand, produce results that are testament to the system's high level of constraint. While in the retro-model, the spatial extent of inundation is visibly increasing with flow, modern conditions show little spatial expansion of inundation. Rather, the constraint of levees throughout the reach has decreased channel capacity and raised flood levels, inherently increasing vulnerability. These results agree with current literature which has found river engineering to be a contributor to increasing flood heights at the reach scale.

Reduced flood peaks and regulated flows after the construction of Cochiti Dam beg the question of whether the flows modeled in this study are plausible. After all, the operations of Cochiti Dam only allow for a maximum release of 142 to 170 m³/s (5,000 to 6,000 cfs) from the reservoir (Richard and Julien, 2003). Statistical analysis of the flow

record at Albuquerque gage shows that the dam has had a twofold impact on streamflow (Table 7). On one hand, the dam regulates the flow of water through the system, preventing the extreme periods of low flow that the Rio Grande experienced historically. On the other hand, the dam has lessened the severity of flood flows by reducing the one-day maximum (annual flood) by 4% (Richard and Julien, 2003).

Table 7: Comparison of mean daily discharges for the Rio Grande before (1943-1974) and after (1974-1995) construction of Cochiti Dam (modified from Richard and Julien, 2003).

Gaging Station	Mean annual flow (m ³ /s)			1-day maximum (m ³ /s)			High pulse duration (days)		
	Pre-dam	Post-dam	Average change	Pre-dam	Post-dam	Average change	Pre-dam	Post-dam	Average change
Albuquerque	28	42	51%	147	141	-4%	11.3	26.1	131%

However, an altered climate suggests possible future conditions not far from the modeled scenarios in this study. Expected increases in wildfire occurrences and extreme rainfall events pose a serious threat to floodplain communities by increasing the rate of runoff and soil erosion (Gould et al., 2016). In order to capture wildfire effects on sediment yield and erosion rates, future models should incorporate the complex dynamics of sediment transport. Post-fire impacts stretch beyond burn sites, as peak flow magnitudes can significantly increase downstream as a result of decreased vegetation cover and increased surface repellency (Gould et al., 2016). This is of particular concern for the Albuquerque reach of the Middle Rio Grande in that increased stormwater runoff rates from burn scar areas would be routed through the North Diversion Channel, putting the village of Corrales located at the outlet and Albuquerque located downstream at direct risk for flash flooding. Despite this increased vulnerability,

levees continue to provide a false comfort to infrastructure in the floodplain as much of the levee system is lacking in terms of standardization and compliance.

Attempting to mitigate model limitations opens many opportunities for future work. Acquiring more SCS survey line data would allow for modeling of a larger extent of the historical reach. Running the models under unsteady-flow conditions and using the metrics developed in Appendix D would more accurately represent river flow processes like flood wave attenuation and back-water effects (Remo and Pinter, 2007). The fact that the current models do not account for sediment transport or groundwater-surface water interactions directly impacts results and has implications for properties such as turbulence as well as processes involving the availability of energy and river-floodplain connectivity.

The outcomes of this paper are meant to encourage a three-part mindset for river and floodplain management: reconstruct the past, reevaluate current practices, and revise future plans. Reconstructing historic conditions plays a vital role in expanding the current understanding of how systems have changed over time. Only by reevaluating our current practices can we plan for optimal revitalization of natural processes. Current policies do not mandate for laws benefiting nature alone unless there is also a clear benefit to humans. Consequently, water resource managers must rely on environmental services as a means of quantifying the potential impacts of not addressing threats (e.g., cost of flood damage to infrastructure in high risk areas) in order to advocate for the benefits of restoring natural processes. The holistic methodology in this study suggests that issues related to water resources management

are best addressed using an integrative approach. In terms of management, long-term thinking should extend not only into the future, but also into the past. Long-term thinking should be the goal, rather than the limitation.

8 Conclusion

The Middle Rio Grande has experienced a long history of river engineering and land use changes as a result of rapid agricultural and urban development within the floodplain. This study recreates the Albuquerque reach as it was circa 1918 using geospatial reconstruction methods for representing floodplain topography, channel characteristics, and land cover. While current literature on the historical Rio Grande focuses primarily on channel planform adjustments, this study broadens that focus by addressing flood trends with a more holistic approach in considering both land use and topographical changes. Comparing hydrodynamic models for historic and modern conditions shows a significant decrease in inundated area across a range of potential flow scenarios. This proves that river engineering has impacted flooding in the reach and indicates a loss of channel-floodplain connectivity due to channel modifications. This extreme variance from the river's natural response to flooding implies the need for water resources management to focus on restoring ecosystem services such as flood wave attenuation and boosting ecosystem resiliency.

Appendices

Appendix A: Historical Photography



Figure 21: Central Avenue Bridge on May 26, 1930 (from Daves, 1994).



Figure 22: Submerged area five miles north of Socorro, N.M. (from Bloodgood, 1930).



Figure 23: Waterlogged Middle Rio Grande Valley in 1928. Photo taken in Albuquerque near Rio Grande Blvd NW, north of I-40 (from MRGCD, 2009).

Appendix B: Map and Plots of SCS Survey Lines

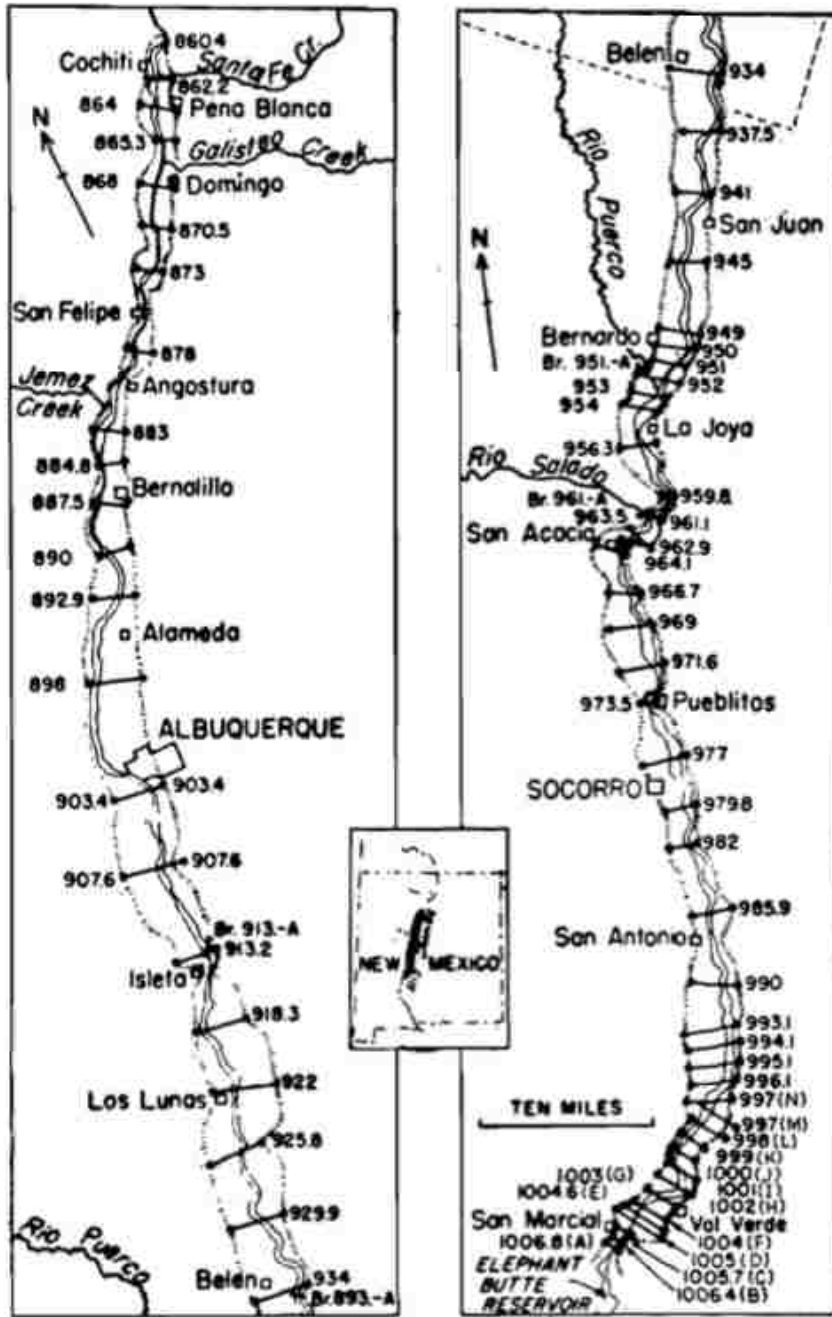


Figure 24: Map of the SCS cross-section range lines located within the Middle Rio Grande Valley, including two range lines in the study reach: 903.4 and 907.6 (from Happ, 1948).

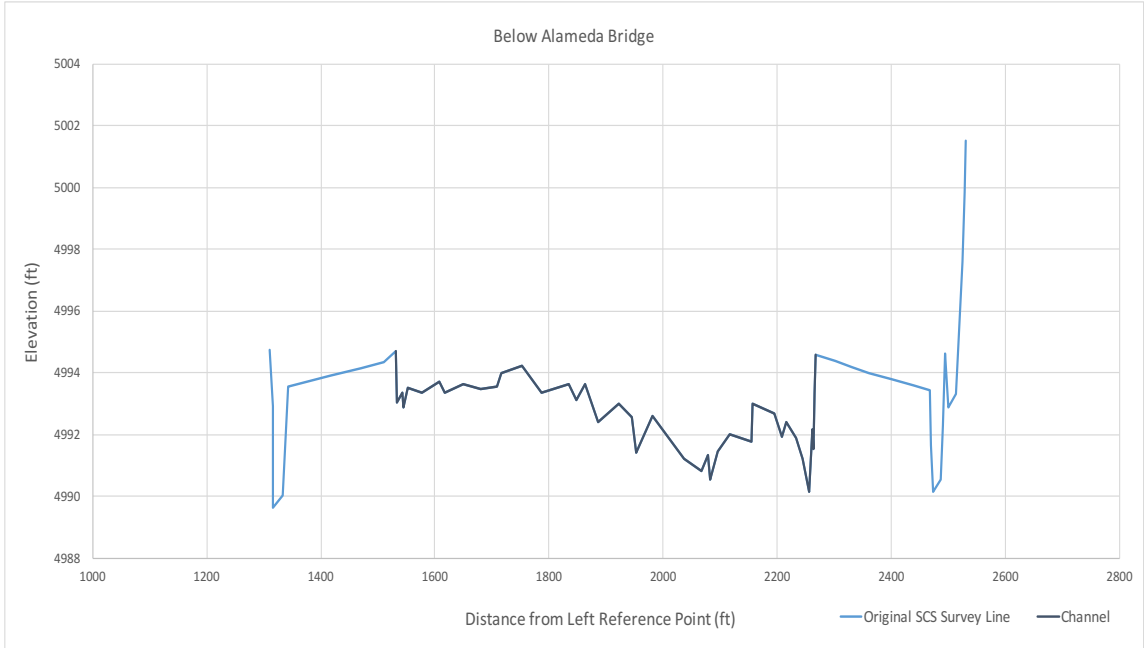


Figure 25: “Below Alameda Bridge” SCS range line obtained from USBR.

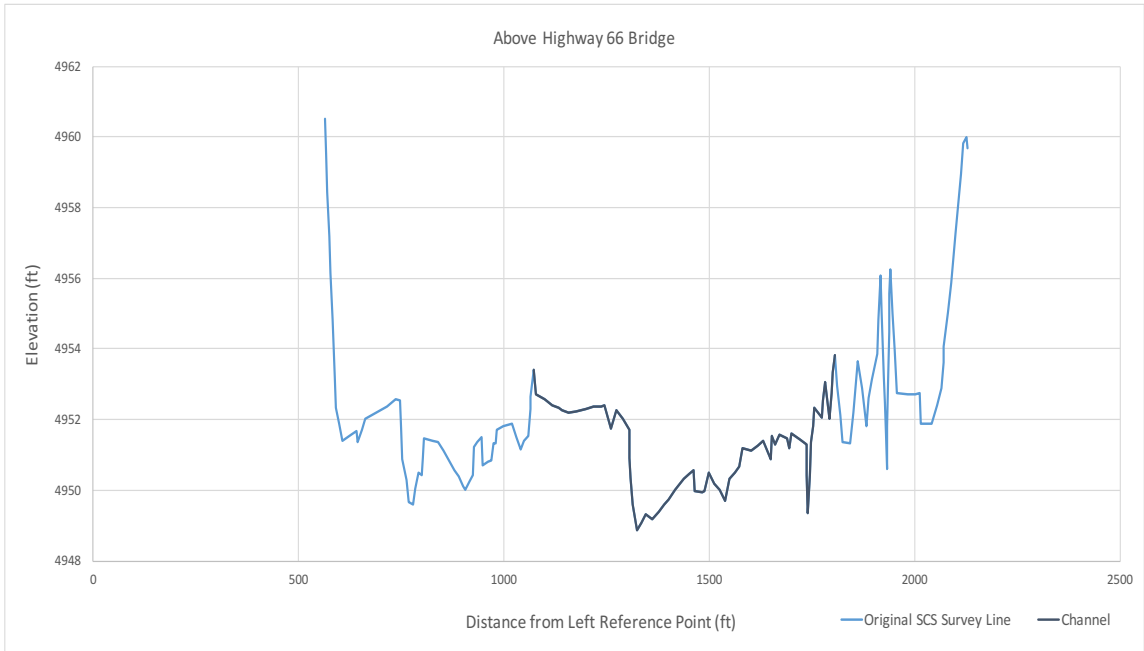


Figure 26: “Above Highway 66 Bridge” SCS range line obtained from USBR.

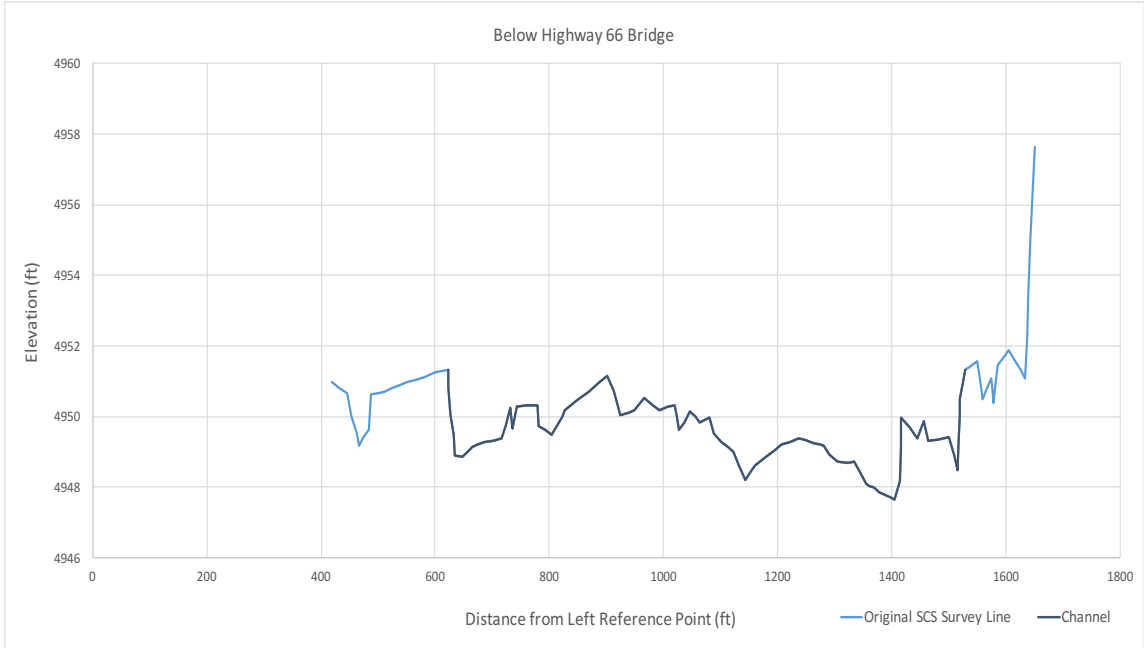


Figure 27: “Below Highway 66 Bridge” SCS range line obtained from USBR.

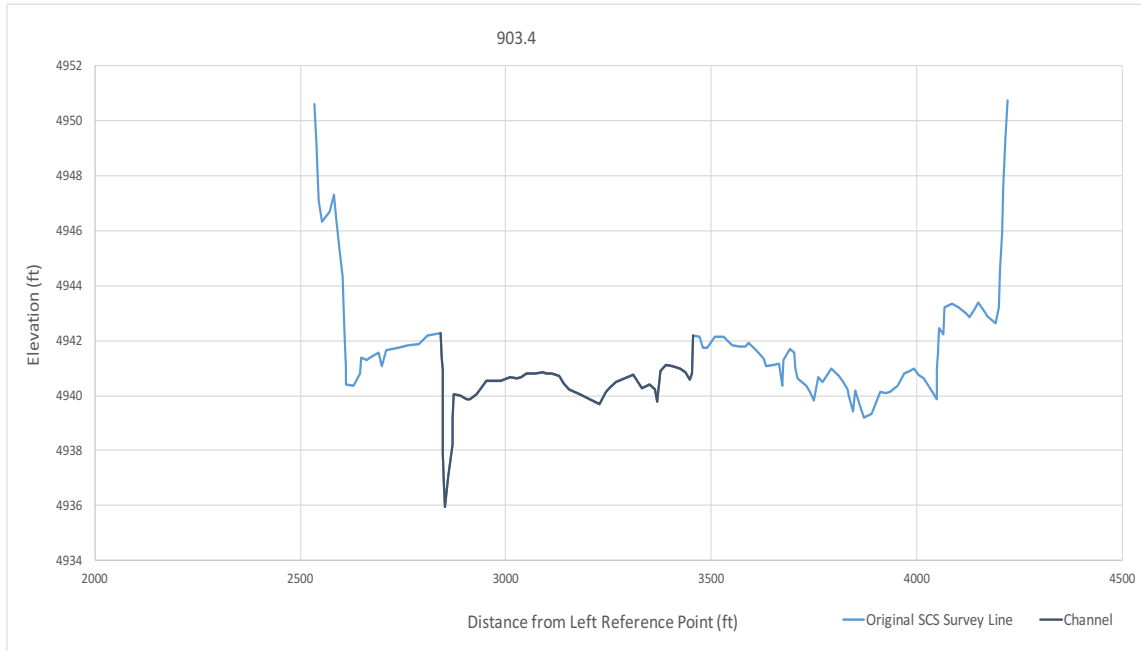


Figure 28: “903.4” SCS range line obtained from USBR.

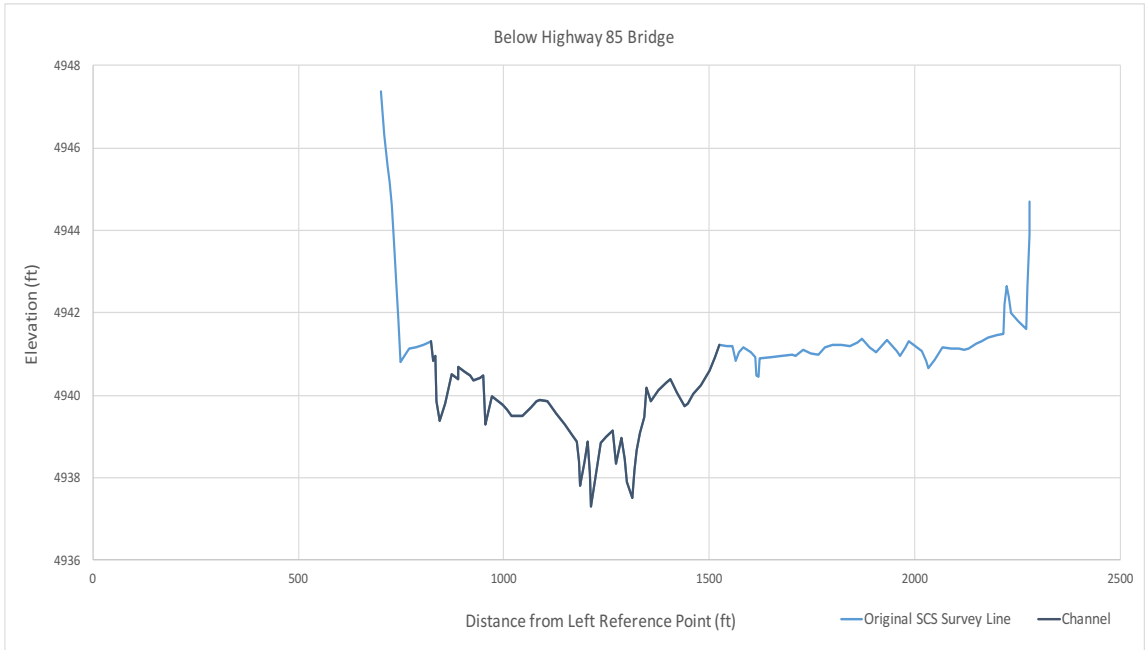


Figure 29: “Below Highway 85 Bridge” SCS range line obtained from USBR.

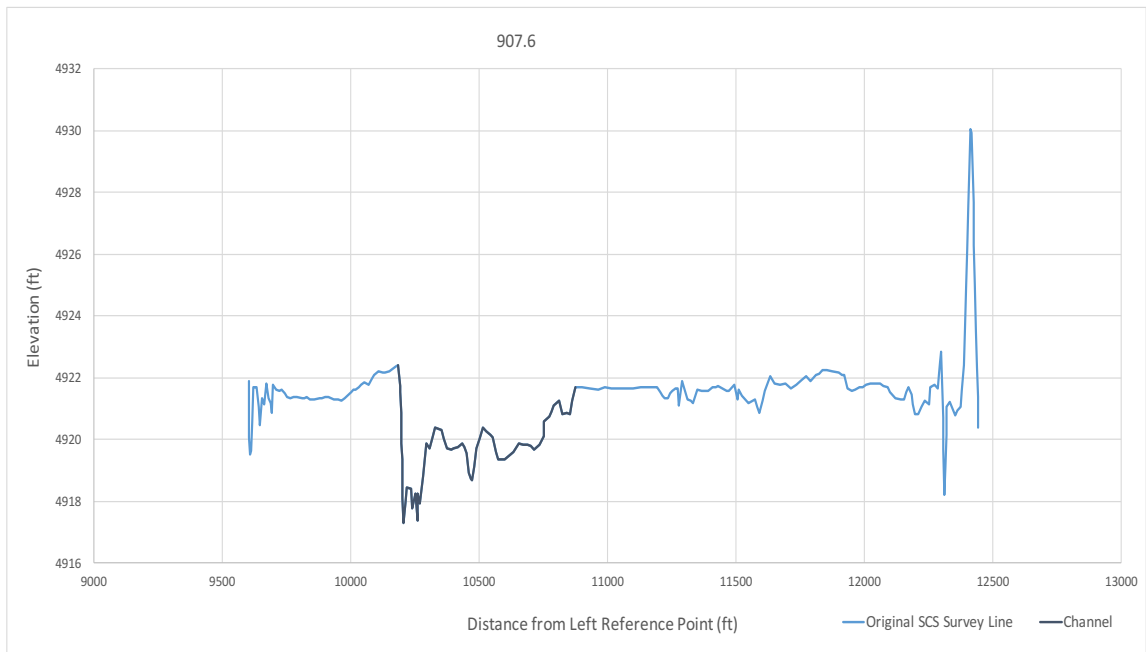


Figure 30: “907.6” SCS range line obtained from USBR.

Appendix C: MATLAB Code

The following code is an example used for SCS cross-section survey “907.6” from the Excel file named “XS_Creation.xlsx”. The code fits the cross-section survey line to the defined channel and generates XY-coordinates for survey points along the channel.

```
% Import survey data from Excel file. Each sheet is named according to
% the cross section survey data it contains. Cross sections are
% surveyed from left to right bank.
% Define Excel file and sheet with cross section being evaluated.
Data=xlsread('XS_Creation.xlsx','907.6');

% Define variables for the column that contains the survey station
% data as well as the first row and the last row to be read.
first_row = 11;
last_row = 75;
column = 10;

% Get linear array of scaled stations (SS). Survey stations are scaled
% to fit the channel width and adjusted to start at 0.
SS = Data(first_row:last_row, column)';

% Get XY-coordinates for left (X_L and Y_L) and right (X_R and Y_R)
% bank points as identified by the user in GIS.
X_L = Data(1,6);
X_R = Data(1,8);
Y_L = Data(2,6);
Y_R = Data(2,8);

% Get width of channel at cross section location as measured by the
% user in GIS.
W_Channel = Data(4,6);

% Generate scaled XY-coordinates for the cross section survey fit to
% the channel using scalevalues, a helper function that scales the
% coordinates based on the defined channel width.

% Scale X-coordinates
X_values = scalevalues(X_L,X_R,SS,W_Channel);
X_column = X_values';

% Scale Y-coordinates
Y_values = scalevalues(Y_L,Y_R,SS,W_Channel);
Y_column = Y_values';

% Get adjusted cross section survey elevations from Excel sheet.
% Elevations are adjusted by a fixed value to set the survey into
% the channel.
Z_adjusted = Data(first_row:last_row,12);

% Combine XYZ data into a 3 column matrix.
xyz = [X_column Y_column Z_adjusted];

% Write XYZ data to tab-delimited text file.
dlmwrite('9076.txt',xyz,'delimiter','\t','precision','%3f');
```

The following code is the scalevalues function used to generate XY-coordinates for the cross-section survey line after being scaled to fit the define channel width.

```
% User defines inputs then the function generates coordinates for each
% survey point as a percent of the distance it lies along the
% cross-section survey line placed within the channel.
function coords = scalevalues(Leftbank, Rightbank, SS, W_Channel)
difference = Rightbank - Leftbank;
[~, columns] = size(SS);
xy_coords = [];
for i=1:columns
    percent = SS(i)/W_Channel;
    value = percent*difference;
    left = value + Leftbank;
    xy_coords = [xy_coords, left];
    coords = xy_coords;
end
```

Appendix D: 2D Hydrodynamic Modeling with D-Flow Flexible Mesh

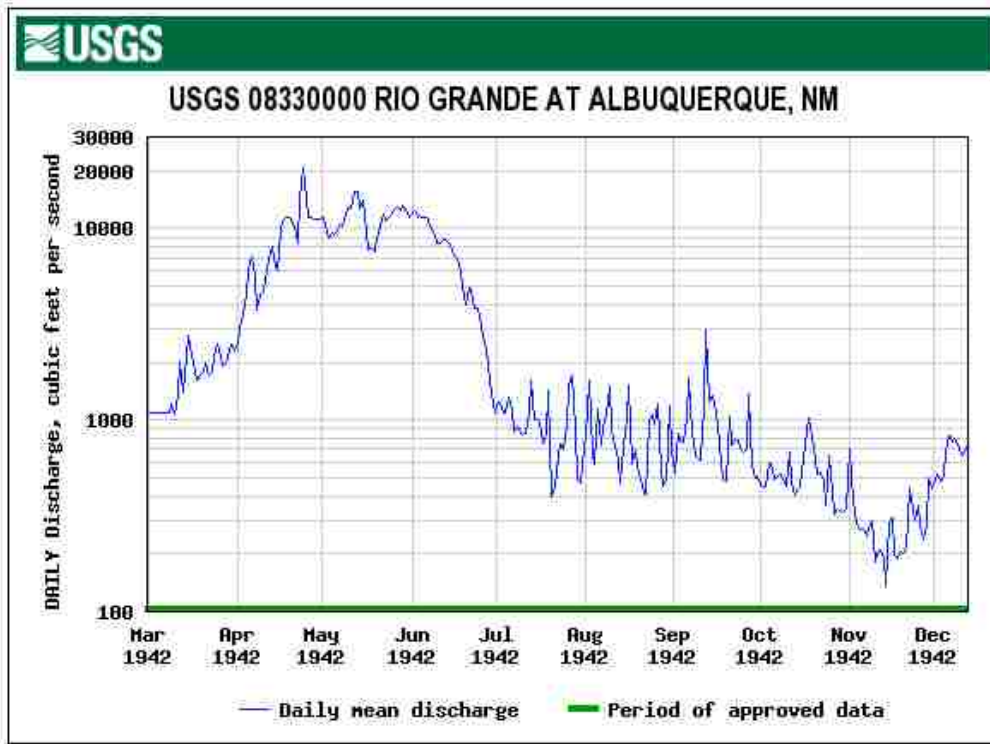


Figure 31: USGS gage data for the 1942 flood used for modeling (from USGS, 2016).

Future work may include a metric-based quantitative approach to analyzing modeling results. Data from D-Flow FM computations are written to NetCDF files at user-defined time intervals. Monitored time series data include water level and velocity at observation stations as well as discharge at cross sections. MATLAB is used to display variables contained within the NetCDF files and extract desired data. Two variables that best characterize the movement of flood waves include: discharge (Q) and water-surface elevation (WSE). Therefore, these variables are used in developing evaluation metrics for quantifying historical engineering effects. First, the relative attenuation ratio (RAR) as shown in Equation 2 is an indicator of the amount of input flow that reaches a location downstream. As the RAR increases, attenuation decreases, and a ratio of one

indicates no attenuation. Equation 3, the relative stage ratio (RSR), compares water-surface elevations at steady peak flow to local water-surface elevations under unsteady flow conditions.

$$RAR = \frac{Q_{pk}^{local}}{Q_{pk}^{up}} \quad (2)$$

$$RSR = \frac{WSE_{local}}{WSE_{Q_{pk}}} \quad (3)$$

where:

Q_{pk}^{local} = peak discharge at downstream location

Q_{pk}^{up} = peak discharge at upstream boundary

WSE_{local} = local stage at unsteady flow conditions

$WSE_{Q_{pk}}$ = local stage at steady peak flow

References

- Bloodgood, D.W. (1930). The ground water of Middle Rio Grande valley and its relation to drainage. New Mexico State College, Agricultural Experiment Station Bulletin 184.
- Bormann, H., Pinter, N., & Elfert, S. (2011). Hydrological signatures of flood trends on German rivers: Flood frequencies, flood heights and specific stages. *Journal of Hydrology*, 404(1), 50-66.
- Chow, V.T. (1959). *Open-Channel Hydraulics*. New York: McGraw-Hill.
- Daves, G. (1994, November). History of Water Development in the Middle Valley. In *The Water Future of Albuquerque and Middle Rio Grande Valley: Proceedings of the 39th Annual New Mexico Water Conference*. Albuquerque, New Mexico.
- Deltares. (2014). D-Flow Flexible Mesh: user manual. Version 1.1.113, Delft, The Netherlands: Deltares.
- Gould, G. K., Liu, M., Barber, M. E., Cherkauer, K. A., Robichaud, P. R., & Adam, J. C. (2016). The effects of climate change and extreme wildfire events on runoff erosion over a mountain watershed. *Journal of Hydrology*, 536, 74-91.
- Happ, S. C. (1948). Sedimentation in the Middle Rio Grande Valley, New Mexico. *Geological Society of America Bulletin*, 59(12), 1191-1216.
- Hink, V.C., & Ohmart, R. D. 1984. Middle Rio Grande Biological Survey. Submitted to the U.S. Army Corps of Engineers, Albuquerque District. Contract # DACW47-81-C-0015.
- Hohensinner, S., Habersack, H., Jungwirth, M., & Zauner, G. (2004). Reconstruction of the characteristics of a natural alluvial river–floodplain system and hydromorphological changes following human modifications: the Danube River (1812–1991). *River Research and Applications*, 20(1), 25-41.
- Jacobson, R.B., Lindner, G., and Bitner, C.J. (2015). The role of floodplain restoration in mitigating flood risk, Lower Missouri River, USA, in Hudson, P.F., and Middlekoop, H., eds., *Geomorphology and Management of Lowland Floodplains: North American and European Fluvial Systems in an Era of Global Environmental Change*: New York, NY, Springer.
- Leon, C., Julien, P. Y., & Baird, D. C. (2009). Case study: equivalent widths of the middle Rio Grande, New Mexico. *Journal of Hydraulic Engineering*, 135(4), 306-315.

- Massong, T., Makar, P., & Bauer, T. (2010). Planform Evolution Model for the Middle Rio Grande, NM. In *Proceedings of the 2nd Joint Federal Interagency Conference, Las Vegas, NV*.
- Middle Rio Grande Conservancy District (MRGCD). (2009). Conservancy District Ditch Banks: Unspoiled Beauty. *Conservancy Today*. Retrieved June 2, 2016, from <http://www.mrgcd.com/uploads/pressrelease/e5a734ab24bb45a79ee0f9765fe65d2c/mrgcd.pdf>
- Mussetter Engineering, Inc. (MEI). (2002a). Geomorphic and Sedimentologic Investigations of the Middle Rio Grande between Cochiti Dam and Elephant Butte Reservoir. Submitted to New Mexico Interstate Stream Commission.
- Mussetter Engineering, Inc. (MEI). (2002b). Hydraulic and Sediment Continuity Modeling of the San Joaquin River from Friant Dam to Mendota Dam, California. Prepared for the U.S. Bureau of Reclamation, Fresno, California, Contract No. 98-CP-20-20060, August.
- Novak, S. J. (2006). *Hydraulic modeling analysis of the Middle Rio Grande River from Cochiti Dam to Galisteo Creek, New Mexico* (Doctoral dissertation, Colorado State University).
- Owen, T. E. (2012). *Geomorphic Analysis of the Middle Rio Grande–Elephant Butte Reach, New Mexico* (Doctoral dissertation, Colorado State University).
- Paz, A., Bravo, J., Allasia, D., Collischonn, W., & Tucci, C. (2010). "Large-Scale Hydrodynamic Modeling of a Complex River Network and Floodplains." *J. Hydrol. Eng.*, 10.1061/(ASCE)HE.1943-5584.0000162, 152-165.
- Pinter, N., & Heine, R. A. (2005). Hydrodynamic and morphodynamic response to river engineering documented by fixed-discharge analysis, Lower Missouri River, USA. *Journal of Hydrology*, 302(1), 70-91.
- Pinter, N., Jemberie, A. A., Remo, J. W., Heine, R. A., & Ickes, B. S. (2010). Cumulative impacts of river engineering, Mississippi and Lower Missouri rivers. *River Research and Applications*, 26(5), 546-571.
- Remo, J. W., & Pinter, N. (2007). Retro-modeling the Middle Mississippi River. *Journal of Hydrology*, 337(3), 421-435.
- Remo, J. W., Carlson, M., and Pinter, N. (2012). Hydraulic and flood-loss modeling of levee, floodplain, and river management strategies, Middle Mississippi River, USA. *Natural hazards*, 61(2), 551-575.

- Richard, G., & Julien, P. (2003). Dam impacts on and restoration of an alluvial river-Rio Grande, New Mexico. *International Journal of Sediment Research*, 18(2), 89-96.
- Rijke, J., van Herk, S., Zevenbergen, C., & Ashley, R. (2012). Room for the River: delivering integrated river basin management in the Netherlands. *International journal of river basin management*, 10(4), 369-382.
- Salazar, C. L. (1998). *Morphology of the Middle Rio Grande from Cochiti dam to Bernalillo bridge, New Mexico* (Doctoral dissertation, Colorado State University).
- Soil Survey Division Staff. (1914). Soil Survey of the Middle Rio Grande Valley Area, New Mexico. Soil Conservation Service. U.S. Department of Agriculture.
- Swanson, B. J., Meyer, G. A., & Coonrod, J. E. (2011). Historical channel narrowing along the Rio Grande near Albuquerque, New Mexico in response to peak discharge reductions and engineering: magnitude and uncertainty of change from air photo measurements. *Earth Surface Processes and Landforms*, 36(7), 885-900.
- U.S. Geological Survey (USGS). (2016). National Water Information System data available on the World Wide Web (USGS Water Data for the Nation), accessed May 24, 2016, at URL http://nwis.waterdata.usgs.gov/nwis/dv/?dd_cd=03_00060_00003&format=img_default&site_no=08330000&begin_date=19420301&end_date=19421212.
- Van Cleave, M. (1935). Vegetation changes in the Middle Rio Grande Conservancy District. Thesis, University of New Mexico, Albuquerque.
- Vorogushyn, S., & Merz, B. (2013). Flood trends along the Rhine: the role of river training. *Hydrology and Earth System Sciences*, 17(10), 3871-3884.
- Yang, Y., Zhang, S., Yang, J., Chang, L., Bu, K., & Xing, X. (2014). A review of historical reconstruction methods of land use/land cover. *Journal of Geographical Sciences*, 24(4), 746-766.
- Zhu, T., Lund, J. R., Jenkins, M. W., Marques, G. F., & Ritzema, R. S. (2007). Climate change, urbanization, and optimal long-term floodplain protection. *Water Resources Research*, 43(6).